DEVELOPMENT OF AN INTEGRATED SENSOR SYSTEM FOR AUTOMATED ON-THE-SPOT MEASUREMENT OF PHYSICAL SOIL PROPERTIES

Pierce Dias Carlson

Department of Bioresource Engineering

Faculty of Agricultural and Environmental Sciences

McGill University

Montreal, Quebec, Canada

February 2021

A Thesis submitted in partial fulfillment of the requirements for the degree of Master of Science.

ABSTRACT

Soil physical characteristics are a major indicator of soil fertility and play a key role in agricultural management decisions. Compacted soils can impact plant growth and affect the workability of the soil for tillage operations. Precision agriculture seeks to detect soil zones with similar characteristics and apply management practices specific to those zones. As precision agriculture technologies are more widely adopted across the globe, collection of the data to drive these control systems is becoming increasingly required. Commercially, only a few devices are directed at measuring soil physical properties. Even fewer attempt to apply an automated principle to the collection of data, reducing the time and labour costs associated with conventional soil data gathering. This research seeks to fill this gap by developing a sensor system to directly measure soil physical properties when combined with an automated vehicle, such as Bearcub 24 (Ztractor, Inc, Palo Alto, CA, USA), or equivalent. The sensor system features a cone penetrometer with separate cone and shaft measurements, an air permeameter and CO_2 sensor, and a generic apparent electrical conductivity, volumetric water content, and temperature sensor. Testing of the sensor system on a Gator vehicle resulted in several performance issues due to the vehicle's light suspension and exhaust fumes. The cone penetrometer demonstrated the capability of generating detailed soil profiles and the combined system was able of estimate soil bulk density with reasonable confidence. Further development of the soil sensor system and autonomous electric tractor will allow for dependable measurements of soil physical properties without human involvement, saving time and money while improving the efficacy of proximal soil sensing.

RÉSUMÉ

Les caractéristiques physiques du sol sont un indicateur majeur de sa fertilité et jouent un rôle clé dans les décisions de gestion agricole. Les sols compactés peuvent avoir un impact sur la croissance des plantes et affecter la maniabilité du sol pour les opérations de travail du sol. L'agriculture de précision cherche à détecter les zones de sol présentant des caractéristiques similaires et à appliquer des pratiques de gestion spécifiques à ces zones. Alors que les technologies d'agriculture de précision sont de plus en plus adoptées dans le monde, la collecte de données pour piloter ces systèmes de contrôle devient de plus en plus nécessaire. Dans le commerce, seuls quelques appareils sont destinés à mesurer les propriétés physiques du sol. Encore moins nombreux sont ceux qui tentent d'appliquer un principe automatisé à la collecte de données, réduisant ainsi le temps et les coûts de main-d'œuvre associés à la collecte conventionnelle de données sur les sols. Cette recherche vise à combler cette lacune en développant un système de capteurs pour mesurer directement les propriétés physiques du sol lorsqu'il est combiné à un véhicule automatisé, tel que le Bearcub 24 (Ztractor, Inc, Palo Alto, CA, USA), ou équivalent. Le système de capteurs développé comprend un pénétromètre à cône avec des mesures séparées du cône et de l'arbre, un perméamètre à air et un capteur de CO2, ainsi qu'un capteur générique de conductivité électrique apparente, de teneur en eau volumétrique et de température. Les essais du système de capteurs sur un véhicule Gator ont donné lieu à plusieurs problèmes de performance dus à la suspension légère et aux gaz d'échappement. Le pénétromètre à cône a démontré sa capacité à générer des profils de sol détaillés et le système combiné a pu estimer la densité apparente du sol avec une confiance raisonnable. La poursuite du développement du système de capteurs de sol et du tracteur électrique autonome permettra d'effectuer des mesures fiables des propriétés physiques du sol sans intervention humaine, ce qui permettra de gagner du temps et de l'argent tout en améliorant l'efficacité de la détection proximale du sol.

ACKNOWLEDGEMENTS

I would like to thank Ztractor, Inc. for making this project possible. Special thanks to Bakur Kvezereli, Stefan Marjanovic, and Charlotte Chapellier of ZTractor for their assistance throughout the project. I would also like to thank Dr. Chandra Madramootoo for his valuable expertise as a supervisory committee member.

Dr. Viacheslav Adamchuk has been an influential and guiding figure for me over the course of my master's degree. His wisdom and generosity helped to guide me throughout this project and our discussions have been invaluable. Thank you to Scott Manktelow for always having a solution to machining problems and teaching me so much over my six years at McGill.

I would also like to thank my lab mates and friends; Roberto Buelvas, Maxime Leclerc, John Lan, and Ann Pille for answering my questions and helping in the field no matter the weather!

I am thankful to my parents and siblings for supporting me throughout my endeavours, and to Sophie Courtemanche-Martel for her steadfast support.

Partial funding for this research project was provided by the Mitacs Accelerate International program and NSERC Discovery.

CONTRIBUTION OF AUTHORS

Bakur Kvezeleri, CEO and Co-founder of Ztractor Inc, expressed the need for an autonomous measurement platform to accompany their Bearcub 24 autonomous electric tractor. The author of this work was responsible for the corresponding research, design, fabrication, and evaluation of the autonomous sensor system. The author wrote the present document. Dr. Viacheslav Adamchuk acted as the project supervisor, where he contributed his wealth of experience and knowledge to the design and evaluation of the sensor system. Dr. Adamchuk is the primary reviewer and editor of this manuscript. At the time of writing Dr. Adamchuk is a professor and chair of the Department of Bioresource Engineering in the Faculty of Agricultural and Environmental Sciences at McGill University.

TABLE OF CONTENTS

LIST OF TABLES

LIST OF FIGURES

LIST OF ACRONYMS

BD – Bulk Density

CAD – Computer Aided Design

DAQ – Data Acquisition

DLCP – Dual Load Cell Penetrometer

EC_a – Apparent Soil Electrical Conductivity

ER – Electrical Resistivity

FDR – Frequency Domain Reflectometry

GCR – Galvanic Contact Resistance

GPS – Global Positioning System

GWC – Gravimetric Water Content

LiDAR – Light Detection and Ranging

PC – Personal Computer

PID – Proportional, Integral, Derivative

PR – Penetration Resistance

PWM – Pulse Width Modulation

RTK – Real Time Kinematic

SMF – Soil-Metal Friction

TDR – Time Domain Reflectometry

UAV – Unmanned Aerial Vehicle

UTC – Coordinated Universal Time

VWC – Volumetric Water Content

1. INTRODUCTION

Agriculture is in the midst of a technological revolution, with precision agriculture allowing for the consideration of spatial and temporal variability in soil and crop factors in nearly every field process. Global positioning systems (GPS), advanced computing and microprocessors, and telecommunications have advanced the capabilities of the agricultural industry to achieve low-input, high-efficiency operations (Zhang et al., 2002). The driving force in precision agriculture is the data which guides management practices and variable-rate technology. This data is collected through a number of methods, including yield sensors built into combines, unmanned aerial vehicles (UAV) drones collecting crop data, satellite imagery, and soil sensors included in traditional implements. These data collection methods have a variety of accuracies and often require significant financial investments for the equipment or analysis of data. Recent technological advancements in the field of autonomous mechatronic systems and sensors have provided opportunities for soil data collection, analysis, and interpretation to be revolutionized.

In general, autonomous control systems in agriculture are included in the navigation systems of vehicles and in implement control. Autonomous vehicle navigation systems offer many advantages over human-controlled systems, with real time kinematic GPS (RTK-GPS) providing precise positioning and guidance within the field. Autonomous navigation systems allow for precise movement so as not to disturb the growing area while operating on a predetermined course. Additional navigation technologies such as machine vision can allow autonomous vehicles to travel completely independent of a human operator while avoiding obstacles and navigating a path of its own volition. Autonomous implements such as variable-rate applicators allow for variable application of field processes as a result of on-board processors, sensors, and actuators. The combination of autonomous vehicles and implements leads to the duplication of many sensors and controllers, which increases costs and reliability issues (Emmi et al., 2014). More recent developments in autonomous systems are striving to better integrate the autonomous implement and vehicle systems such that the respective sensors and control systems work seamlessly to allow for concurrent execution of all automated processes. Development of fully autonomous systems that combine navigation

and implement control have several advantages over the traditional tractor-implement system. Namely, the system can be developed to precise specifications for the task, including reduced weight and size to reduce compaction, with sensor and control systems meeting the specified requirements precisely for the task of interest. Completely autonomous vehicle systems may offer a platform in which newly developed implements incorporate the sensors and processors already on board the vehicle. The sensors on board these autonomous systems or the sensor-equipped implements for which they are paired may help to capture the data necessary for precision agriculture practices.

Currently, there is a lack of effective and economical spatial data collection systems for soil physical properties, and it is possible that this area may be filled by autonomous systems. Soil physical properties are a vital component in understanding crop yield variability. Physical properties such as soil texture, structure, and porosity have a significant impact on water retention, nutrient adsorption, and microbial activity, all of which impact plant growth and yield. Measurement of soil physical properties typically requires proximal sensors for measurement of the soil property using probes or implements that interface directly with the soil. Accurate determination of soil physical properties requires laboratory-based analysis to calibrate the sensor results for the specific soil texture. With completely autonomous vehicles linked to machine learning algorithms, sensor systems may analyse their readings within the field based on calibration models based on historical data within the spatial context.

This project developed an autonomous sensor system capable of capturing a variety of soil physical parameters from which soil bulk density (BD) could be estimated. The system was designed and built for Ztractor Inc. (Palo Alto, California, USA) to interface with their Bearcub 24 model of autonomous electric tractor. The Bearcub 24 and sensor system allow for autonomous measurement of soil characteristics using point-based measurements. The system was to include a dual load cell cone penetrometer and combined air permeameter and CO_2 sensors, as well as an off-the-shelf sensor for soil moisture, temperature, and apparent electrical conductivity. The sensor system was tested in field conditions and compared to reference commercial sensors as well as laboratory measurements of the physical soil properties.

2. LITERATURE REVIEW

2.1 **Automation**

The agricultural industry has been quick to adopt new technologies from other industries while pioneering technologies of its own. One technology that is revolutionizing the agricultural industry in modern times is precision agriculture. Precision agriculture is the management strategy based on data that involves sensors, information systems, machinery, and informed decisions to increase productivity and enhance environmental stewardship. Precision agriculture relies on large amounts of data, of which there remains a need for technology to facilitate the acquisition of spatially related data on crop, soil, and environmental factors (Stafford, 2000). Automation offers promise for its ability to capture a significant amount of spatial data without requiring labour – one of the costliest components of agriculture.

In automating spatial soil measurements, the most common implementation is through stationary sensor installations, such as moisture sensors buried in the soil that capture soil water content throughout a season and transmit data through a wireless network (Adamchuk et al., 2019). The use of a variety of sensors, including soil texture, soil temperature, and soil moisture, has allowed for automated and wide-reaching capture of data that has helped to improve the environmental stewardship of agricultural practices.

Several robots have been developed for the purpose of autonomous field measurements. Scholz et al. created a robot to carry out automated soil penetrometer readings using the BoniRob platform (2014). Their design featured a single cone penetrometer capable of stopping measurements if the resistance exceeded a certain level due to a hard object or extreme compaction. A soil moisture sensor was also included in their design. They found the measurements to be highly accurate with the automatic function working well, and they concluded that any further improvements should include additional sensors to enhance the usefulness of the robot. Iqbal et al. (2020) developed a Multipurpose Autonomous Robot of Intelligent Agriculture (MARIA) system, which featured a 3 degree of freedom manipulator arm fitted with a soil temperature and moisture probe. This platform allowed for autonomous navigation using light detection and ranging

(LiDAR) and measurements of soil properties, with the manipulator arm able to interchange the tools for extraction of samples or integration with other sensors. Lukowska et al. (2019) created a robot with solar power generation and an integrated implement for soil sample extraction. Featuring a drill, vacuum collection, and sample storage, the system was developed with the intention of allowing for autonomous soil sample collection on large-scale farms. Naumov et al. (2019) described a strain gauge assembly integrated into autonomous vehicle chassis which would allow for determination of soil physical characteristics based on stresses on the drivetrain and suspension of the vehicle as it rolled over soil.

Recently, drone network concepts have emerged, with large companies, such as Fendt, working on fleets of automated field robots (AGCO, 2021). While this concept focuses on field operations, such as seeding and applying pesticides, rather than data acquisition, onboard sensors on each vehicle may allow for generation of spatial data. Barrientos et al. (2018) described the Robot Fleets for Highly Effective Agricultural and Forestry Management (RHEA) system, which included various autonomous aerial and ground vehicles fitted with an assortment of sensors to monitor environmental data. Small ground vehicles measured parameters including ground temperature and humidity, which were then broadcast over Wi-Fi to a base station within a greenhouse, allowing continuous operation and measurement in conditions that would not be humanly possible. The unmanned ground vehicle featured a y-axis actuator to raise and lower the temperature and soil moisture sensors into the ground.

Ünal et al. (2020) developed a sensor system combining a cone penetrometer and Werner EC_a array to create an implement that would work in conjunction with an autonomous robot to collect rapid electrical resistivity (ER) measurements in large areas. It featured a single y-axis movement to lower the penetrometer and Werner array to soil level. This measurement platform exhibited the ability to perform autonomous operations while providing ER maps. The developed system showed promise in alleviating the degree of labor associated with the collection, analysis, and interpretation of agricultural data.

2.2 **Proximal Soil Sensing**

The measurement of soil physical characteristics is important in facilitating agricultural processes and natural resource sciences. Soil properties can reveal pertinent information about soil conditions and processes. By measuring soil properties, farmers can make choices that have both environmental and economic benefits. In a study on oil-seed yields in the UK, Halcro et al. (2013) compared fertilizer application schemes based on 3 approaches. The first used a uniform-rate application, the second was based on a fertility-based management zone, and the last was founded on a field map derived from a combined infrared optical probe and load cell to capture soil texture. The fertilizer application based on the third approach, the sensor map, produced the largest yield per hectare, while also using less nitrogen fertilizer. Additionally, with improvements in soil sensing, farmers can adopt agronomic practices that allow for improved carbon sequestration and policies related to field management practices and sustainable development (Rossel & Bouma, 2016).

The sensors used to collect this data vary in function, cost, and ease-of-use, with some sensors operating from the ground, others from unmanned aerial drones or satellites. In general, the measurements must be of high density and number to produce detailed and informative soil maps. Ground-based soil sensors are based on different technologies, including electrical/electromagnetic, electrochemical, mechanical, optical, acoustic, and pneumatic.

Electrical sensors are most often used to capture the soil's apparent electrical conductivity (EC_a). EC_a is the ability of soil to conduct an electrical current and can be used in assessing salinity and soil texture (Adamchuk et al., 2018). There are several sensors available to measure EC_a, including electromagnetic induction (EMI), which uses a transmitter coil to create an eddy current and a receiver coil to measure the induced current within the soil (Adamchuk et al., 2004). The depth and reliability of these sensors is determined by the frequency of the primary field and the distance between the coils. These EMI sensors can be affixed to a three-point-hitch or dragged over the soil on a sled. EMI sensors are lightweight; however, they tend to drift and often require calibration. Another method of measuring EC_a is through

galvanic contact resistivity (GCR), which uses a minimum of 4 electrodes, some that induce a current into the soil and others that measure the potential difference. The configuration of these sensors is typically a towed or three-point-hitch implement consisting of electrode discs. The arrangement of the disks is flexible, with many possible configurations and models available commercially. Despite being cheap, GCR does not work well in dry soils and it is a heavy instrument, which can lead to unwanted soil compaction when taking measurements.

Soil water content can be measured with probes that use the physical properties of water within the soil to reflect and transmit waves. Time domain reflectometry (TDR) is a method of measuring soil water content, in which two or three rods containing a transmission line and wave guide are inserted into the soil (Adamchuk et al., 2018). The probes capture the velocity of propagation from precisely timed impulses that are reflected from the soil back towards the sensor. In wet soil, the velocity of the pulse is slower than in drier soils. These readings are less dependent on texture, salinity, and temperature than other moisture sensors. Another method for soil water content determination is frequency domain reflectometry (FDR). This method calculates the dielectric constant of the soil medium through the propagation of electrical signals at a specific frequency (Ojo et al., 2015). The volumetric water content is derived from the difference between the dielectric constants of water and soil particles. FDR sensors often have temperature sensors built into one of the propagation probes.

Soil structure is an important physical property that influences nearly every other physical property, from water retention and thermal capacity to mechanical impedance. The intrinsic permeability of soil is a measurement that can be used to define soil structure based on the ability of air to flow through the soil pore spaces. Permeability is dependent on the size and continuity of macropores within the soil structure (Fish and Koppi, 2006). Air permeability is also useful in assessing the gas phase movement through soils. Air permeability is most often measured using a laboratory air permeameter. Fish and Koppi (2006) describe an *in situ* air permeameter which involves injection of pressurized CO_2 through a soil tube above the surface, measuring the resulting pressure within the cylinder using a digital manometer. As the soil tube

is sealed on all sides except the bottom circular cross section 50 mm below the soil surface, the CO_2 that is unable to enter the soil registers as an increased pressure on the manometer. They found their air permeameter provided a useful structural index, though sensitive to structural differences of soils under different management practices. Iverson et al. (2001) also describe an *in situ* air permeameter of similar design. Comparison between the *in situ* permeameter and the standard lab permeameter found that care was needed when interpreting the results of the *in situ* sensor, due to the lack of a boundary with which to define air flow after the air has entered the soil, with the geometry of air flow paths within the soil impacting the reading. Nevertheless, using a shape factor model, the permeameter design was able to make reliable *in situ* air permeability measurements. Mohammadi and Vanclooster (2019) describe a similar *in situ* air permeameter design, with the distinction that the air is drawn up through the soil rather than injected from above. This design used a siphon from a water tank to create a vacuum and draw air into the tank from the soil-tube, with pressure measurements at the soil tube stage and at the siphon-exit stage. The advantage of this design is that it does not require pressurized gas or batteries to operate in the field; however it does require a water source to refill the tank. Chief et al. (2006) found that the measured area by permeameters varied significantly in managed, unstructured soils compared to undisturbed soils.

Mechanical sensors can be used to measure soil compaction, which is important for estimating plant growth, erosion, and fuel consumption during tillage (Gebbers, 2014). This soil property can be measured using load cells attached to vertical or horizontal penetrometers, measuring the resistance applied to the penetrometer from the soil (Adamchuk et al., 2018). Horizontal penetrometers are used for on-the-go measurements, dragged behind the tractor using special tines to capture load cell readings at different depths. Cone or vertical penetrometers can take a reading at only one location at a time. Penetrometers permit only small-scale variability in measurement, with factors such as soil moisture and texture affecting sensor readings, making frequent and dense measurements desirable.

Combined sensor systems aim to capture several soil properties at once by using multiple sensors or sensors fused together. The Veris MPS3 (Veris Technologies, Inc., Salina, KS, USA) is an on-the-go sensor system

that combines pH electrodes, an optical sensor, and an EC_a sensor to capture and map soil texture, organic matter, and pH of the soils. The system is a 635 kg three-point-hitch implement. The EC_a sensor used the GCR method, with 6 disks on the implement. Behind the discs is a shoe that collects a soil sample, raises it, where pH electrodes then take readings from the sample, are rinsed with water, and the soil sample is then discarded. At the end of the system is a spectrophotometer used to capture organic matter content. The system can produce pH maps with a high degree of linearity to laboratory values (Schirmann et al., 2011). Issues with this system include the need for field-specific calibration and the build-up/blockage from crop residue on the measuring area. Another combined system that utilizes sensor fusion, is the Veris Profiler 4000 (Veris Technologies, Salina, KS, USA), a combined optical sensor, penetrometer and EC_a sensor. In this sensor, the load cell measures the force required to penetrate the soil with the shaft, while the tip of the shaft acts as an electrode to capture EC_a. A spectrometer built into the tip collects soil spectrum data throughout the length of insertion. Lin et al. (2014) developed a penetration resistance and VWC combined sensor in which a capacitance sensor was built into the penetrometer cone tip, allowing for simultaneous measurement of penetration resistance and water content to predict bulk density. Vaz et al. (2001) developed a cone penetrometer-TDR probe that also allowed for simultaneous measurement of penetration resistance and water content through the soil profile for estimation of bulk density.

2.3 **Targeting Soil Properties**

Bulk density is a vital soil parameter that significantly impacts soil processes. Soil bulk density (BD) is the ratio of the mass of dried soil sample to the volume the solids and porous spaces of the sample occupy (Blake, 1965). High BD typically results in reduced soil porosity due to reduced soil structure. Bulk density can impact root growth due to penetration resistance or even bind nutrients within the soil. When upper soil layers dry out or are compacted, inter-root competition and low influx can reduce plant uptakes of potassium (Seiffer et al. 1995). BD also effects the water movement and aeration within the soil structure. Soil BD can be increased depending on vehicle traffic and soil management methods. For example, strip tillage was found to reduce bulk density compared to conventional tillage, resulting in an increased infiltration rate and

saturated hydraulic conductivity of the soil (Jabro et al., 2011). By adjusting bulk densities through cultivation, farmers can manipulate the available-water capacity and air capacity of soils (Archer & Smith, 1972). Bulk density can also allow for prediction of soil susceptibility to compaction for sandy soils (Saffih-Hdadi et al., 2009). Direct determination of BD requires oven drying of soil cores, and thus can only be estimated through field-based sensors by measuring soil characteristics that relate to BD. The targeted soil properties for the automated sensor system were chosen based on their contribution to estimation of soil bulk density.

Soil water content is an important soil characteristic which is used in the determination of a variety of soil properties, as well as to provide insight into yield estimations and drought/flooding severity among other applications. Specifically, soil water content affects the amount of water and nutrients available to plants, as well as the soil aeration status (Voroney, 2019). Increased water contents indicate that the pore space within the soil is filled with more water than air. Prolonged cycles of wetting and drying of soils can decrease aggregate stability and lead to the collapse of soil pores, and weakening of soil structure (Emdad et al., 2004). Water content can indicate issues with flooding or drying, which may lead to further problems depending on the situation. In some cases, higher water content can undesirably impact crop quality. For example, soil which had lower water contents and organic matter resulted in improved grape performance for cabernet wine production (Cheng et al., 2014). Soil water content measurement is essential for estimations of BD.

Compaction is a problematic soil state that may serve as an indicator for other soil properties, including the penetration resistance of plant roots through soil, hydraulic conductivity, and soil porosity. One method of determining soil compaction is through the measurement of soil penetration resistance (PR) with a cone penetrometer. Several soil parameters are directly correlated to penetration resistance, including bulk density, porosity, water content, matric potential, and soil texture (Vaz et al., 2011). PR can indicate compacted soils, with values larger than 2.5 MPa restricting root elongation. A standardized cone penetrometer measurement includes a 30° cone tip inserted into the soil at 30 mm/s (ASABE Standards,

R2013). Cone penetrometer measurements are comprised of 2 factors: the penetration resistance acting on the cone and the soil friction of the shaft of the penetrometer. PR is highly dependent on the water content within the soil, with higher water content resulting in lower PR. This is the result of the water changing the cohesive properties of the soil. Soil texture also significantly impacts PR readings, with higher percentages of clay resulting in a higher PR. To compare PR more accurately among different soils, Vaz et al. (2011) developed a correction to account for the influence of water content on PR. It is assumed that plant roots experience negligible friction, but the friction component acting on the cone penetrometer accounts for a large proportion of the total resistance to insertion, and it is useful to separate this from the mechanical impedance on the cone to assess the difficulty plant roots may experience in penetrating the soil (Bengough et al., 2008). However, there remains value in the soil-metal friction component for purposes of determining the impact of soil texture and water content on the penetration component. For one, soil-metal friction can be used to determine the spatial variation in soil-tillage adhesion, a large component in the drag force in tillage operations. This force generally follows the simple laws of friction; however there is an additional adhesive component, independent of the normal load (Payne, 1956). Part of the soil-metal friction component includes the adhesive forces of the soil on the solid surface of the shaft. These adhesive forces are composed of Laplace pressure, meniscus tension and viscous resistance (Tong et al., 1994). The water film plays a dominant role in the adhesive forces. Chen et al. (2019) found that the adhesion factor for clay soil is not a fixed value but highly dependent on moisture content. These adhesive effects can affect mouldboard plows, leading to the coating of adhesion resistive materials such as polytetrafluoroethylene (PTFE) to the plows. Azadegan and Massah (2012) found that the adhesion of clay soil to steel decreased as temperature increased. Birch et al. (2016) observed that for the soil types they tested, soil-metal friction increased for all soils with water content up to 20%, with water content above 20% resulting in a decrease in frictional resistance as the increased water content caused the film layer to act more as a lubricant. Additionally, the variation between soil types in frictional resistance increased as the water content increased, with lower water content exhibiting similar adhesion constants. Abbaspour-Gilandeh et al. (2018) observed a similar phenomenon, with the distinction that different soil types reached their respective

maximum soil-metal friction peak at different soil water content levels, before entering a liquid phase where friction was reduced due to a lubricating effect. At water content of less than 10% the forces acting on the tool are purely frictional, followed by an adhesion phase, and then a lubrication phase as water content increases, respectively.

Soil pore space is related to bulk density, representing the total volume occupied by soil pores within a given volume of soil. Macropore percentage and interconnection determine how water is stored and moves through the soil (Voroney, 2019). An abundance of a greater percentage of macropores within soil can be an indicator of healthy biological soil activity including earthworm, fungal, and bacterial activity (USDA, 2008). Additionally, increased pore space and the corresponding improved soil structure can increase the soil water holding capacity. Soil organic matter of a soil is a major contributor to both biological activity and macropore spaces, as organic products bind with soil particles to form aggregates, and create more pore spaces. Tillage of wet soils can destroy the surface structure, so measurements of air permeability can be an indicator of soil structure and the impact of tillage on fields.

Soil CO_2 levels are an indicator of subsurface CO_2 production and transport (Hashimoto & Komatsu, 2006). While CO_2 flux is more commonly referenced in the literature, CO_2 concentration is an equally important parameter. Soil CO_2 concentrations are a function of the depth of the soil. Determination of subsurface concentrations is usually difficult, depending on temperature, with varying porosity and gas diffusivity giving concentrations that could be misleading. Low porosity can result in seemingly high CO_2 concentrations due to low gas diffusivity when point measurements are made, especially at lower depths. Soil CO_2 concentration measurements are usually made with *in situ* permanent sensor installations that record both the subsurface CO_2 concentration and surface flux. The microbial activity and corresponding CO_2 production were observed by Flechard et al. (2007) to positively correlate with soil temperature throughout the day in moderate to high soil water contents along an exponential curve. Drier soils exhibited an inverse relationship, with the highest concentrations in the early morning. Their data suggested that CO_2 built up in the soil at night, with increased atmospheric pressures during the day as a result of wind flushing

the CO_2 from the soil. Lai et al. (2012) found that higher electrical conductivity resulted in significantly reduced soil respiration.

2.4 **Literature Review Summary**

The increased use of variable-rate field management systems relies on the simultaneous development of proximal soil-sensing systems to generate the required data. Conventional proximal sensor systems operate as implements that require an operator's labour and energy while further compacting the soil. While there are commercial sensors that provide multiple soil property measurements in one system, the majority of soil measurement devices are single-property measurement systems. On top of this, there are even fewer systems that operate completely autonomously.

The Bearcub 24 is a novel autonomous electric tractor platform available commercially. While its onboard sensors can provide detailed GPS and optical data as it travels, it does not have a method to directly measure soil characteristics as it travels. To provide a detailed dataset on soil physical properties, implements of equally autonomous function must be developed that will be capable of measuring a multitude of soil properties in conjunction with the Bearcub.

Physical soil properties are of particular interest in the development of autonomous systems. While remote sensing can generally predict soil characteristics through mechanisms such as hyperspectroscopic imaging, measurement of physical soil properties such as BD typically requires proximal sensors or sampling for laboratory analysis. Direct measurement of these physical soil properties is a natural application for autonomous systems, given their light weight and versatility. Automated sensor systems such as these reduce the difficulty associated with collected and analysing soil characteristics, while helping to improve soil health for crop production by allowing farmers to make informed management decisions related to soil physical characteristics.

3. MATERIALS AND METHODS

3.1 **Sensor System Design**

In developing a sensor system capable of providing a broad overview of soil physical characteristics for estimation of bulk density (BD), the sensors were selected such that each could provide data on more than one soil attribute, either through correlation or sensor fusion to measure multiple soil properties. Soil physical characteristics of interest included soil mechanical impedance, soil-metal friction, and soil air permeability. To measure these parameters, the sensor system required a cone penetrometer, air permeameter, and an additional sensor to measure soil volumetric water content (VWC), temperature, and apparent electrical conductivity (EC_a).

3.1.1 Cone Penetrometer

The cone penetrometer design, henceforth known as the dual-load cell penetrometer (DLCP), required three parameters: simultaneous measurement of soil mechanical impedance about the cone tip and soil-metal friction on the shaft, capability of measuring forces up to 6 MPa, and operation in compliance with American Society for Agricultural and Biological Engineers (ASABE) standards (ASABE Standards, R2013). The ASABE standard dictates a 30 mm/s insertion speed, using a 30° cone tip. As the cone tip endures erosive forces, stainless-steel construction was required which could not be fabricated on-site. A commercially available cone tip with a 30° angle could not be sourced, but a 60° cone tip with 1.5 cm^2 area from M&L Testing Equipment Inc (Dundas, Ontario, Canada) was available with accompanying shaft and inner rod. This penetrometer cone and shaft were sourced as replacement parts from a complete digital dynamic cone penetrometer system manufactured by Humboldt Mfg. Co. (HS-4210, Elgin, IL, USA).

Numbers in parenthesis following part descriptions refer to Figure 3.1 labels. A ServoCity (Winfield, KS, USA) 2491 N, 12 V DC heavy-duty actuator (1) was chosen as no other model under consideration could meet the 30 mm/s speed requirement under load. This linear actuator also featured an internal reference potentiometer for determining the position of the cone penetrometer. A Cytron (Penang, Malaysia) 40A 12

V DC motor driver controlled the speed of insertion and direction of the actuator. Two load cells were mounted on the end of the actuator shaft. The first was a 4448 N pancake load cell (3), chosen specifically for its resistance to off-axis loading for longevity, mounted to a custom actuator to a threaded tap adapter (2). A threaded rod (4, center) connects this load cell to an aluminum block assembly. The block assembly consisted of two 127 mm aluminium plates (6,10) held together with steel bolts (4, outer) separated by aluminium spacers (8). A 2224 N button load cell (7) was fixed to the top plate with M4 bolts (5) and nuts (9). Nylon locknuts (11) held this assembly tight. The inner rod of the penetrometer shaft (12) passed through a hole in the lower aluminum plate to contact the button load cell. The outer shaft of the cone penetrometer (13) screwed into the bottom plate. The cone tip comprised two parts: a threaded shaft (14) and a captive bolt with the cone on the end (15).

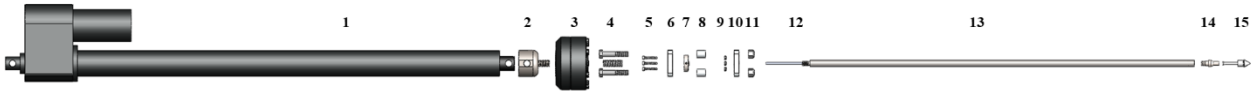

Figure 3.1 Dual Load Cell Penetrometer (DLCP) exploded view

This configuration allowed the mechanical impedance on the cone to be measured directly by the 2224 N button load cell, while the entire force on the penetrometer was transmitted to the 4448 N pancake load cell. By subtracting the force of mechanical impedance from the total force, the forces on the penetrometer shaft could be determined.

The reference potentiometer proved too noisy for proportional, integral, and derivative (PID) control of the penetrometer speed, but calibration indicated that the actuator was powerful enough for the compaction level of the tested soils to maintain a 30 mm/s speed over varying forces when fed a calibrated pulse width modulation (PWM) signal from the controller. For logging the depth of measurements, the reference potentiometer worked without any issues.

3.1.2 RK520-02 Soil Moisture Sensor, Temperature and EC

For measurement of soil temperature, VWC, and EC, a variety of sensor types were considered, including a dedicated time domain reflectometry (TDR) system and thermistor. In the end, a combined frequency domain reflectometry (FDR) and thermistor sensor was chosen. The RK520-02 Soil Moisture Sensor, Temperature and EC_a Probe (Rika Sensor, Changsha, China) was an inexpensive, small-format sensor with sufficient technical specifications for agricultural purposes. Stainless-steel probe material provided moderate resistance to repetitive insertion movements and the low cost allows for easy replacement on the sensor system. The sensor was mounted on the end of a linear actuator with a 200 mm-stroke using a 3D printed adaptor. Set screws kept the RK520 secured within the adaptor.

3.1.3 Air Permeameter and CO_2 Concentrations

For measurement of soil air permeability, the idea of combining air permeability measurements with the extraction of soil vapours was considered. To accomplish this, a system was designed which combined low-pressure vapour sample extraction using a syringe, and high-pressure injection using compressed air.

Numbers in parenthesis following part descriptions refer to Figure 3.2. The basis for the probe was a stainless-steel soil vapour extractor probe tip (1). This probe tip featured 16 holes grouped in four sets of four, spaced evenly in vertical rows. The probe was supported by a steel connector (3) which allowed for a connection to a linear actuator and the rest of the air sensor. This connector had an additional support structure (6) to support the probe during insertion as the probe was offset from the actuator shaft. A soft plastic seal (2) ensured the probe was airtight between the insertion hole and soil. A pneumatic cylinder (7) was

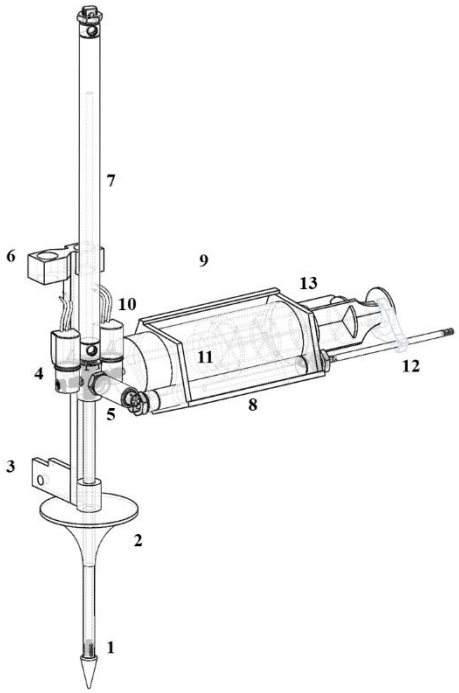

Figure 3.2 Air permeameter and soil CO_2 sensor

normally extended the entire inner length of the probe tip to reduce the amount of ambient air in the system prior to measurement. CO_2 extraction began with the pneumatic cylinder retracting, a solenoid valve (10) opening, allowing air to enter the syringe apparatus (9). The syringe was opened by way of another pneumatic cylinder (8) connected to the syringe plunger (13) with an adapter (12). This was supported by a welded steel frame. Mounted on the bottom of the syringe plunger was a CozIR-A CO_2 sensor (11) (CO2Meter Inc, Ormond Beach, FL, USA). Once a sample has been drawn, the solenoid valve (10) closed, and CO_2 concentrations were logged in ppm every half-second over a 10 second interval. Meanwhile, the other solenoid valve (4) opened, and air was injected into the system at 414 kPa. Air was generated from a VIAIR100C (VIAIR, Irvine, CA, USA) 12V DC air compressor which fed a 3.78 L tank. The compressor was switched on by a pressure switch which turned on at 550 kPa and off at 690 kPa. The tank also fed two 5 port/2-position solenoid valves which control the pneumatic cylinders. Injection pressure was regulated via a pressure regulator valve which maintained constant input pressure into the system over a 4 second interval. The resulting pressure was recorded with a 690 kPa gauge pressure transducer over 5 s, to include pressure before and after injection. All connections had NPT threads and were sealed with Teflon tape. The sensor was controlled via an Arduino Uno (Arduino, Somerville, MA, USA) connected to a relay board, which opened and closed the four solenoid valves. The Arduino received instructions from the main sensor system computer. The available air within the tank was enough to facilitate one measurement between refilling of the tank. Cycling of the air within the syringe and sensor occurred once the probe has been removed from the soil after the measurement. Air was injected into the probe to clear any soil that may have entered the inlet holes as well as to clear out the previous sample. This cycling action released enough air to drop the tank below 550 kPa, triggering the compressor to fill the tank in preparation for the next measurement.

This configuration allowed for pressure measurement dependent on the soil's ability to be permeated with high-pressure air. Soils with low air-permeability would lead to a quicker build-up of air and thus a higher

pressure within the probe during injection. Soils with high air-permeability would expect more air to flow out of the probe resulting in a lower pressure measurement.

3.2 **System Design**

3.2.1 Frame and Structural Design

Considerations for design of the sensor system included overall weight, distance of probe insertion from Bearcub 24 (Ztractor Inc., Palo Alto, CA, USA) tracks, and the mechanism for which the probes would position themselves above the soil. To reduce complexity, a system was designed in which the sensor structure rotates about a pivot point such that the probes can be oriented perpendicular to the ground during measurement and then be lifted away for transport as depicted in Figure 3.3.

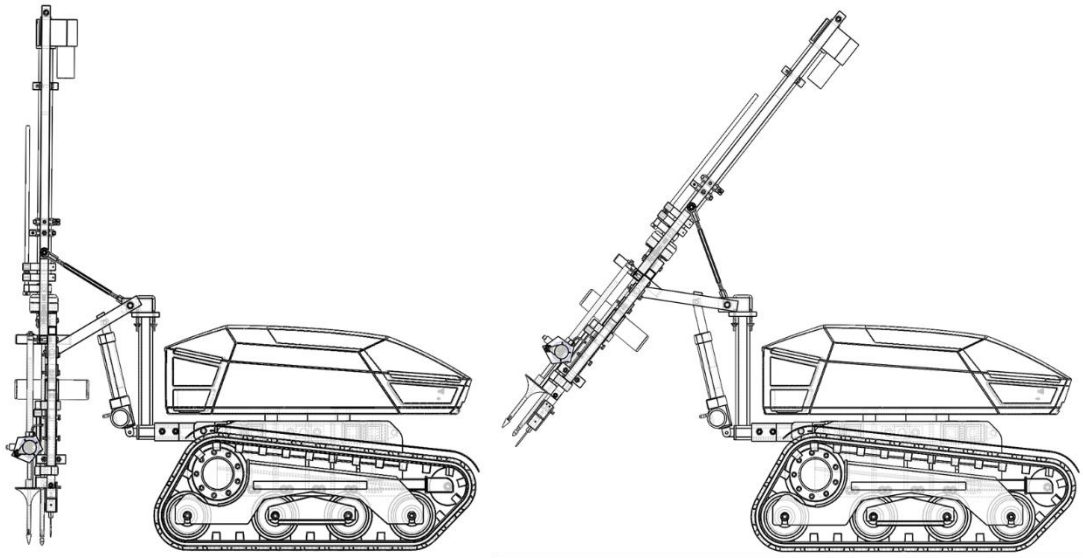

Figure 3.3 Bearcub 24 and sensor system in measurement (left) and travelling (right) positions

Numbers in parenthesis following part descriptions refer to Figure 3.4. Dimensions can be found in Appendix A. The sensor system can be divided into three main sections: the straight hitch (1) and pivot point bar (2) made up the Bearcub adapter section. The 50-mm steel square-tube straight hitch (1) interfaced with the Bearcub's class 3 straight hitch receiver, which then connected to the lift actuator (5). At the top of this L-shaped piece, the pivot point bar (2) was secured with rectangular U-bolts, where several connections were made to the second main section: the linkages. The linkage section was comprised of a

steel H-shaped lower-linkage (4) secured to the pivot point bar by lift pins (13). The lift actuator (5) was connected to the center of this lower linkage. The top linkage (3) was comprised of two turnbuckle-style

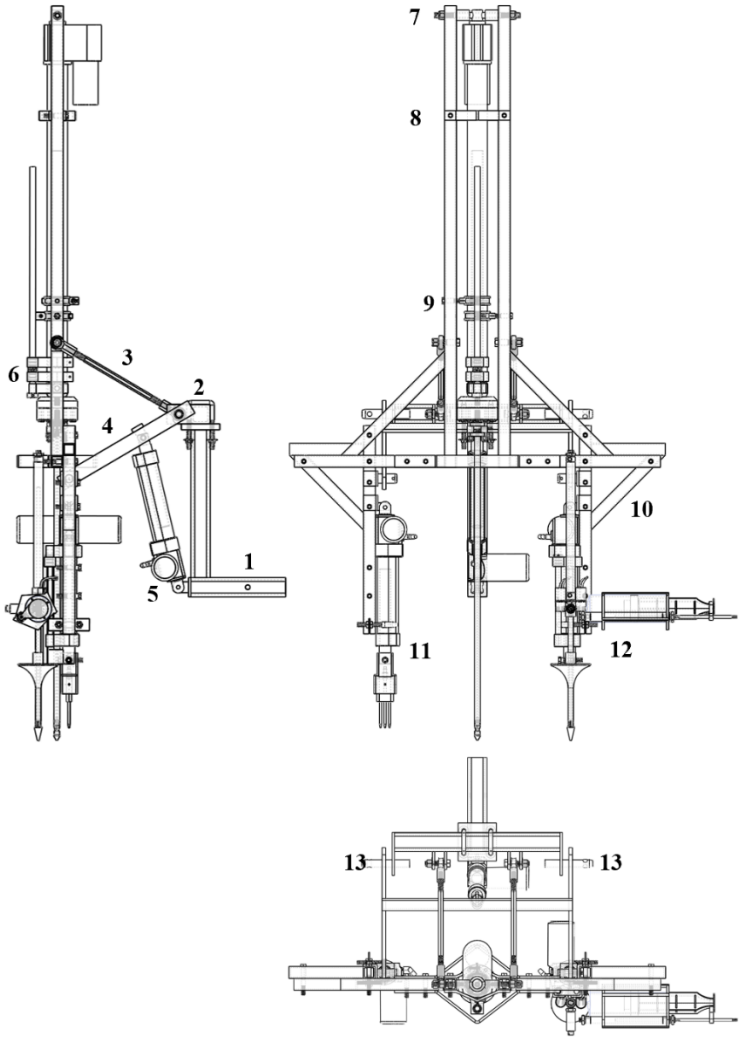

Figure 3.4 Side(left), front(center), and top(bottom) profiles of sensor system

connectors, which allowed for adjustment of the angle of the probes relative to the soil in the measurement position. The last and most complex section was the sensor frame. Made from 31 mm-aluminum-square tubing, it was broken into 4 L-shaped sections with reinforcing bars (10). The frame was intentionally divided into these separate pieces to facilitate shipment for this research project. The two sides were joined by bent steel pieces at the top (8) and middle. Centered in the sensor frame was the cone penetrometer actuator, secured with a 12.7 mm bolt at the top (7). Rubber pipe clamping hangers (9) helped to support the actuator and allowed for adjustment of left-right orientation. Satellite actuators were mounted on the

left and right lower aluminum frames using fabricated adapters. These actuators supported the RK520-02 (11) and CO_2/Permeameter (12). Not pictured are the compressor and air tank, which were mounted on the bottom linkage.

3.2.2 Electrical system

When mounted on the Bearcub 24, the sensor system was powered with 12 V DC sourced from the Bearcub's internal batteries. When used as a standalone unit, the sensor system was wired as seen in Figure 3.5 with a 12 V DC battery in place of the Bearcub power. Power was routed through a fuse box to the individual components of the system. The 4 actuators were controlled through Cytron DC motor drivers (MDS40B and MD20B, Cytron Technologies, Penang, Malaysia), which allowed for PWM control of

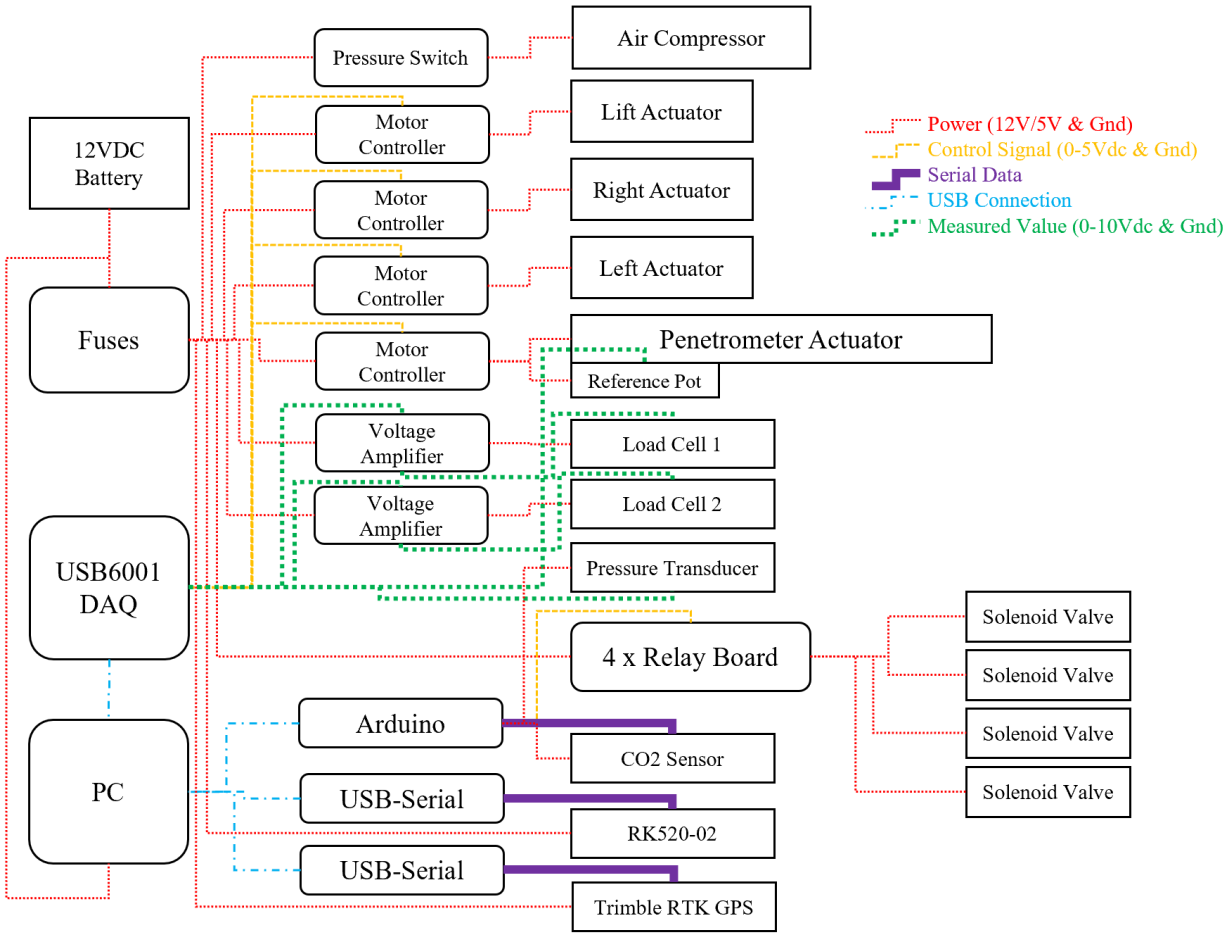

Figure 3.5 Connection diagram of sensor system electrical and signal components

motor speed. A NI USB 6001 data acquisition (DAQ) device (NI, Austin, TX, USA) served as the control source for the motor drivers. The RK520-02 was connected over a USB-Serial cable to the Windows PC (Surface Book 2, Microsoft Corp, Redmon, WA, USA). The load cell measurements were passed through Load Cell Central TLE voltage amplifiers (Load Cell Central, Milan, PA, USA) which then connected to the DAQ. The pressure transducer was supplied 5V DC power by the Arduino for the air and CO_2 sensor, with the reference signal connecting to the DAQ. All sensor grounds were connected to a DAQ ground pin so that voltage measurements were made with respect to a common ground. The Arduino was powered over USB from the PC.

3.3 **Software Design**

3.3.1 Python implementation and Sequence

The sensor system was controlled by a Python 3.8.1 script (Appendix B) written and executed in Microsoft Visual Studio Code 1.53.1 (Redmond, WA, USA) running on a Windows 10 64-bit PC. A python-library specific to the NI USB-DAQ facilitated simple integration of motor control and reading of sensor values. Threading was used to divide each sensor sequence into an individual sequence that could be run simultaneously by allocating a CPU thread to each sequence. Geospatial data was obtained from a Trimble AgGPS 542 (Trimble LLC, Sunnyvale, CA, USA), with the receiver mounted on the top of the sensor system, and the base station located on a nearby building. Flow of the initialization sequence and subsequent sensor threaded sequences is illustrated in Figure 3.6. An entire measurement sequence took 75 s to complete. When the system was powered on and the program was started, the first task the system ran through was the initialization of ports. This involved opening serial ports for the Arduino, GPS, and RK520-02 sensor, as well as creating the necessary tasks for each channel on the DAQ. Once finished, the channels on the DAQ instructed the linear actuators to reset their positions to 0, and then return to the default initialization position for travel. When a start command was received, the three separate threads for each sensor/actuator were started. The penetrometer began immediately to make full use of all the current available from the battery. Once it reached either a depth of 600 mm or 1870 N, it stopped and retracted.

After this delay, the two other actuators lowered their sensors into the ground. This delay also helped to ensure that any erratic movement resulting from the penetrometer did not impact the seal the air permeameter created with the soil as it entered. The two sensors begin their respective sequences and are retracted once finished. Before the lift actuator returned the system to its travelling orientation, it checked that the actuators had been fully retracted so as not to lift the system with probes still in the soil. If any actuators were detected remaining in the ground, the system sent a command to retract them again. If this failed as well, the system could alert the operator of a failure.

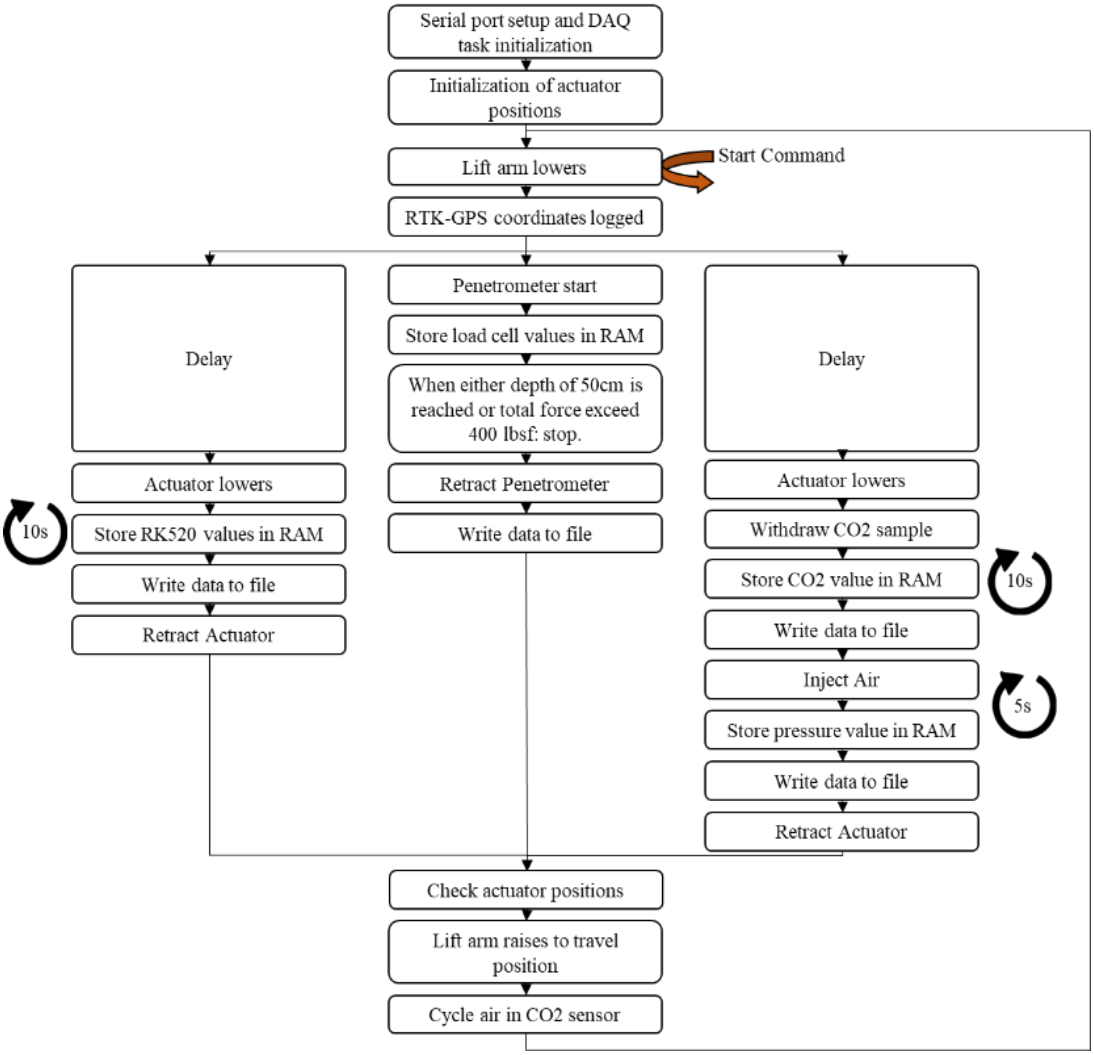

Figure 3.6 Python sequence of sensor system

Data was initially stored in the random access memory (RAM) and was only written to the unicode text file upon exiting the sensor sequence to ensure that threads did not try to access the text file at the same time, and so that any delay caused by writing to the file did not interrupt the timing of the reading.

3.3.2 Data Logging

The initial setup of the sensor system as a standalone unit from the Bearcub 24 meant that data logging would be done on the same computer running the Python program. Data was logged for each sensor using a unique descriptor tag to identify the source sensor for the data point. RTK-GPS coordinates and Coordinated Universal Time (UTC) linked individual sensor measurements from the same measurement point. GPS coordinates from the global positioning system fix data (GGA) sentence were left in NMEA-0183 format. Additional timestamps were recorded the exact moment a measurement is taken from the system clock.

Measurements for the cone penetrometer were logged on a new line for each new depth. Each line included the penetration depth in cm, penetration resistance in MPa, and the shaft friction in N. Data from the RK520-02 was logged line by line over the 10 s recording interval, allowing for post processing in case of erroneous values. This line included the EC_a, temperature, and moisture measurements. The air and CO_2 sensor measurements were broken into two separate sensor identifiers. The CO_2 concentration was logged line by line over the 10 second measurement period. Air injection pressure was logged in 10 Hz intervals over the 4 s injection period. All values were comma-separated for easy manipulation in post-processing. An example of the sentence fields shared between different sensor outputs can be seen in Table 3.1.

Table 3.1 Common fields in sensor comma separated sentence output, with example (common fields in bold)

Common Field	**Meaning**
*Example: PT,**2020-11-06,13:41:13,08:41:28,4524.83111078N,07356.50258244W,37.763,m,** 21.4,cm,PR,0.50,MPa,SF,15.2,lb,*	
2020-11-06	UTC Date
13:41:13	UTC time for beginning of measurement – common in all sentences for a measurement
08:41:28	System time at generation of sentence
4524.83111078N	Latitude
07356.50258244W	Longitude
37.763,m	Altitude

The fields unique to each sensor are detailed in Table 3.2, where decimal values were truncated for readability. Note how the UTC time for each sensor type is the same, whereas the system time varies.

Table 3.2 Unique fields in sensor comma separated sentence output, by sensor with example (unique fields in bold)

Unique Field	**Meaning**
PENETROMETER	
*Example: **PT**,2020-11-06,13:41:13,08:41:28,4524.83111078N,07356.50258244W,37.763,m,* ***21.4,cm,PR,0.50,MPa,SF,15.2,lb,***	
PT	Sensor identifier
21.4,cm	Depth of reading
PR,0.50,MPa	Penetration resistance, value in MPa
SF,15.2,lb	Shaft Friction, value in lbf
RK520-02	
*Example: **RK**,2020-11-06,13:41:13,08:41:32,4524.83111078N,07356.50258244W,37.763,m,* ***EC:,0.245,dS/cm ,Moisture:,0.0,% ,T:,13.1,C,***	
RK	Sensor identifier
EC:,0.245,dS/cm	EC, value in dS/cm
Moisture:,0.0,%	Moisture, value in g/g
T:,13.1,C	Temperature, value in Celsius
CO_2	
*Example: **CO2**,2020-11-06,13:41:13,08:41:37,4524.83111078N,07356.50258244W,37.763,m,* ***652,mg/kg,6.0,s,***	
CO2	Sensor identifier
652,mg/kg	Concentration of CO_2 in mg/kg
6.0,s	Seconds since beginning of measurement
AIR PERMEAMETER	
*Example: **AP**,2020-11-06,13:41:13,08:41:58,4524.83111078N,07356.50258244W,37.763,m,* ***4.83,psi,0.05,s,***	
AP	Sensor Identifier
4.83,psi	Pressure value in psi
0.05,s	Seconds since beginning of measurement

3.3.3 Bearcub 24 Integration

Though not developed in the scope of this project, the sensor system may be entirely integrated into the Bearcub 24 NVIDIA Jetson computer (NVIDIA, Santa Clara, CA, USA). GPS data would come from the Bearcub 24's onboard RTK-GPS, and data would be immediately logged, processed, and made available through the Bearcub 24's cloud service. The additional sensors on the Bearcub 24 would allow it to observe and choose adequate measurement locations. The sensor system and production Bearcub 24 can be observed in Figure 3.7.

Figure 3.7 Render of Ztractor Inc. Bearcub 24 and sensor system in travelling position

3.4 **Field Testing**

3.4.1 Test Site

Field testing was conducted at the Macdonald Campus Farm located in Ste-Anne-de-Bellevue, QC, Canada, depicted in Figure 3.9. The principal field used was a 12 ha forage field growing a combination of grass and clover, which can be seen in Figure 3.9 relative to the farm extent. In this area, there are principally mineral soils with a loam texture as illustrated in Figure 3.8. Testing was done in October 2020 post-

mowing and post-harvest, respectively, several days after rainfall. The local fall season was relatively wet, resulting in the field soil water content being relatively saturated.

Figure 3.9 Satellite map of farm and field extents on the western tip of the Island of Montreal (Source: Google maps, 2021: online)

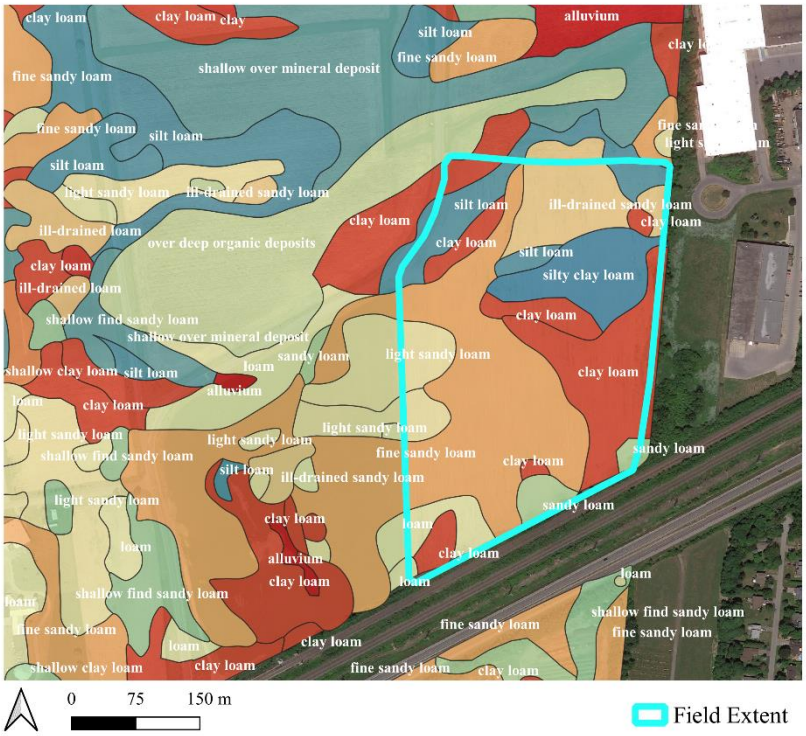

Figure 3.8 Soil texture classification of field and surrounding farm from Macdonald Campus Soil Classification Survey (Source: Google Maps, 2021: online)

3.4.2 Testing Method

For this test, the sensor system was mounted on the back of a John Deere Gator 850D XUV (John Deere, Moline, IA, USA) The system can be seen mounted on the Gator and on the Bearcub in Figure 3.10.

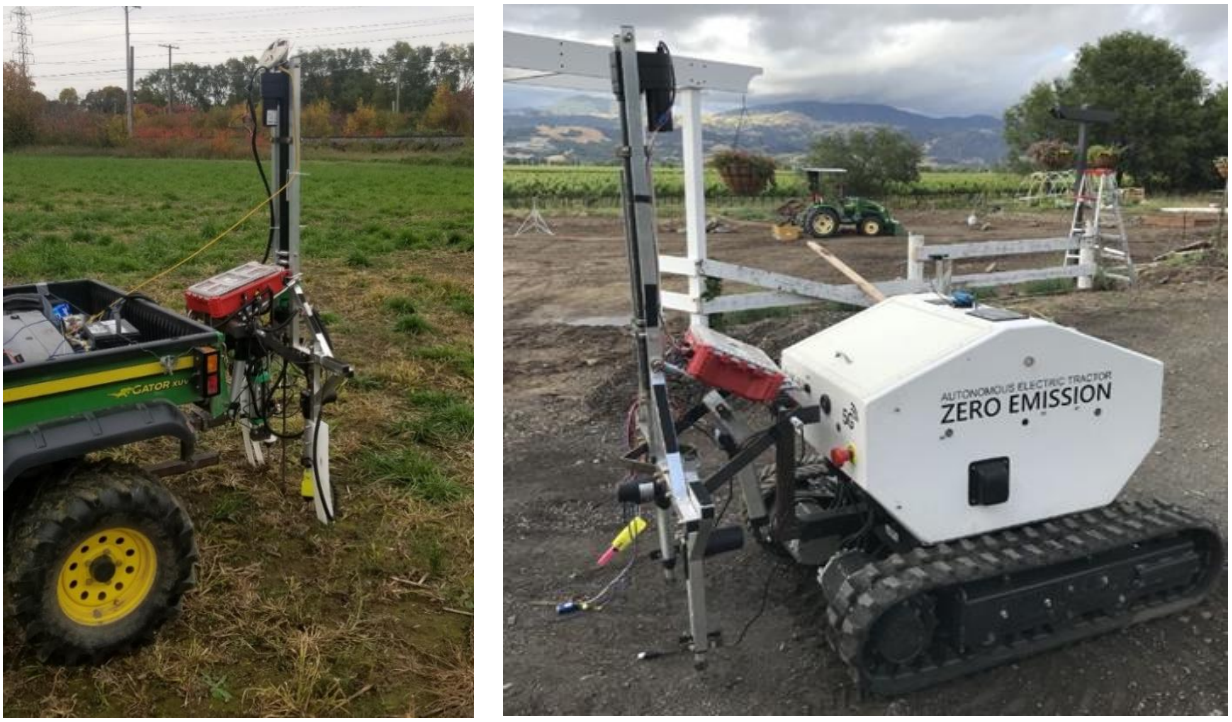

Figure 3.10 Sensor system mounted on the John Deer Gator Vehicle (Left) and Bearcub 24 Prototype (Right) (Source: Pierce Dias Carlson 2020)

Two sets of data were collected for two separate field tests. The first was a rapid collection of measurements with the objective of generating spatial maps of the measured parameters, for comparison with high-density EC_a measurements obtained using EC Quad-1000 (Veris Technologies Inc., Salina, KS, USA) and elevation data. This dataset was taken entirely within the field extent, with points marked in Figure 3.11.

The second set of data was used for direct comparison of sensor values with conventional measurement techniques. For each spatial point in which the sensor system recorded data, several reference sensors were used to record values. To compare VWC, a Field Scout TDR 300 (Spectrum Technologies Inc., Bridgend, UK) was used. For temperature and EC, a Field Scout EC 110 (Spectrum Technologies Inc., Bridgend, UK) was used. To compare compaction profiles, a Field Scout SC900 (Spectrum Technologies Inc.) was used. Additionally, a soil core was taken using an aluminum cylinder with an inner diameter of 83 mm and a

length of 76 mm, hammered into the soil with a rubber mallet. To increase the variability in soil densities, several points in adjacent fields used for soy and corn production were measured also, as depicted in Figure 3.11. The soil cores were dried in an oven at 105 °C for 4 days and weighed, allowing for laboratory determination of gravimetric water content (GWC), bulk density (BD), and VWC. The insertion for each reference sensor relative to the sensor system probes are shown in Figure 3.12. Locations were chosen such that the reference measurement would be near the sensor system probe of similar characteristic, without being so close as to cause disturbance as in the case of the soil core and two penetrometer holes.

Figure 3.11 Location of measurements for laboratory and FieldScout comparison (top), and measurements for spatial comparison (bottom) - not all points are georeferenced. (Source: Google Maps, 2021: online)

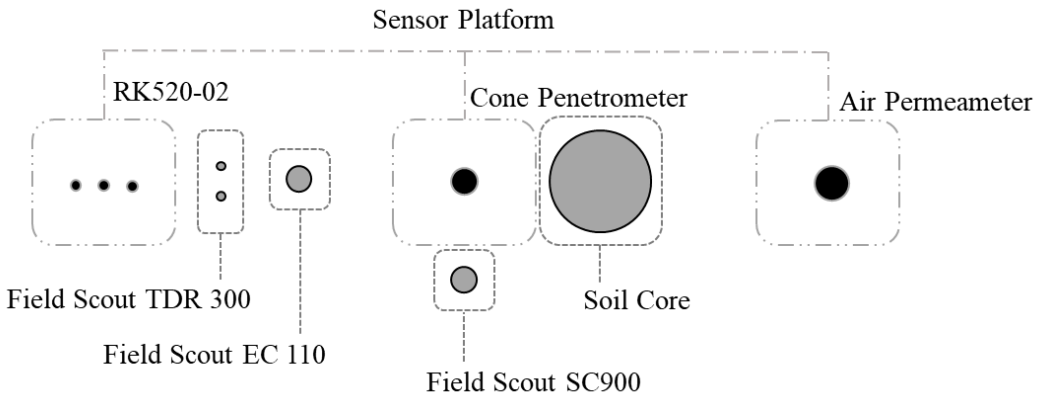

Figure 3.12 Spatial layout of sensor system probes and handheld reference sensors

The collected data is presented in Appendix C and was used to perform several assessments as detailed in Table 3.3. The first assessment addressed the functionality of the sensor system, particularly the autonomous function and overall durability. Additionally, each sensor was compared to its commercial handheld counterpart. Pearson correlations between all sensors and laboratory values were checked to determine existing relationships. For correlations of note, statistical significance was checked with F-tests based on 0.05 confidence level. Additionally, a multivariate regression analysis was performed wish SAS GLM (SAS Institute Inc., Cary, NC, USA) to evaluate the efficacy of the measured values in estimating soil bulk density.

Table 3.3 Analysis of parameters

Prediction Value	Predictor	Model	Justification
Dataset 1 – Map Comparison			
Historical Veris Quad EC1000	*RK520-02 EC_a*	*Spatial trend comparison*	Capability of RK520 to generate EC_a map
Elevation	*RK520-02 moisture*	*Spatial trend comparison*	Relation of soil moisture to elevation
Elevation	*Penetrometer shaft friction*	*Spatial trend comparison*	Relation of shaft friction to moisture through elevation
Dataset 2 – Laboratory Comparison			
Bulk density (lab)	*All sensor values*	*Multivariate regression*	Efficacy of sensor system to estimate soil bulk density
Gravimetric water content (Lab)	*Penetration resistance*	*Exponential regression*	Determine soil-water component of PR
Bulk density (Lab)	*Penetration resistance*	*Exponential regression*	Determine BD component of PR
Gravimetric water content (Lab)	*Penetrometer shaft-friction*	*Linear regression*	Determine soil-water component of shaft-friction
Bulk density (Lab)	*Penetrometer shaft-friction*	*Linear regression*	Determine BD component of shaft-friction
Bulk density (lab)	*Air permeability*	*Linear regression*	Determine BD component of air permeability
Volumetric water content (Lab)	*Air permeability*	*Linear regression*	Determine soil-water component of air permeability
Volumetric water content (lab)	*RK520-02 VWC*	*Linear regression*	Determine accuracy of RK520-02 sensor
Dataset 2 – FieldScout Comparison			
FieldScout TDR200	*RK520-02 VWC*	*Linear regression*	Compare sensor measurements
FieldScout EC110 EC	*RK520-02 EC*	*Linear regression*	Compare sensor measurements
FieldScout EC110 Temp.	*RK520-02 temperature*	*Linear regression*	Compare sensor measurements
FieldScout SC900	*Penetration resistance*	*Visual comparison*	Compare sensor measurements
RK520-02 VWC	*Air permeability*	*Exponential regression*	Investigate correlations
Penetrometer Shaft-Friction	*Air permeability*	*Linear regression*	Investigate correlations

4. RESULTS AND DISCUSSION

4.1 **Autonomous Functionality and Reliability**

The sensor system performed reliably throughout the experiment. The autonomous function was only tested insofar as the system was able to perform the measurement on its own when given the signal. As such, the only interaction between operator and sensor system was the initiation of a sequence. When mounted on the Bearcub 24 (ZTractor Inc, Palo Alto, CA, USA), the Bearcub 24 would have autonomous control over when to send a signal to commence the measurement. Though used only for operator convenience, the sensor system demonstrated the capability of returning the status of the system as it performed its function, which could easily be adapted to integrate with the Bearcub both for vehicle-sensor communication and to provide remote status updates to the operator.

A major issue arose during the initial testing and experimental measurements with regards to the JD Gator vehicle on which the sensor system was mounted. The extremely light rear suspension was initially engaged when the system was mounted, dropping the rear of the vehicle by roughly 200 mm due to the weight of the system itself. Actuation of the cone penetrometer resulted in the rear of the vehicle being lifted into the air when more compact soils were encountered due to the reduced load on the suspension. This caused unwanted flexing of the penetrometer shaft as the lift movement was angular to the front wheel. If the rear of the vehicle lifted high enough, the sensor system would be lifted as well, which could result in the two satellite probes being displaced from the soil. Because the force was not necessarily exceeding that of a solid object such as a stone, the penetrometer's auto-stop function would not engage, continuing to lift the rear of the vehicle into the air. Over time this would result in deformation of the shaft or potentially complete breakage of the shaft. Additionally, as the rear of the vehicle is lifted into the air, the depth and the contact of the cone penetrometer are affected, which could impact the reliability of measurements. Weights could not be added to the bed of the Gator vehicle, as this would further engage the suspension, reducing the clearance of the sensor system and preventing it from orienting itself perpendicular to the ground. This

phenomenon would not be expected on the Bearcub 24, for which the sensor system was originally designed, as the straight hitch, frame, and drivetrain are rigidly fixed together and the center of gravity of the 498 kg Bearcub has been considered in the design. Initial testing of the sensor system during development was conducted on a pickup truck with weights in the bed. Due to the comparatively solid nature of the straight hitch in this configuration, the system performed without issue; thus, this issue is only of relevant concern when the sensor system is on a vehicle with a light suspension.

The system was otherwise rigid and endured the stresses of repeated insertions well. Most of the measurement time was occupied by the non-cone penetrometer actuators travelling very slowly when moving the system up and down and inserting probes into the soil, due to their slow maximum speed.

4.1.1 Cone Penetrometer

The cone penetrometer exhibited the capability to generate a comprehensive dataset of soil profiles as illustrated in Figure 4.1. The system was able to measure compacted soils up to 6 MPa depending on the defined maximum force threshold. The weakest point in the assembly is where the penetrometer shaft meets the aluminum load cell block, as the penetrometer shaft is reduced to a 1.4 mm wall thickness for its upper mating threads. A reinforcing tube should be added here to provide additional support in case of bending. The auto-stop function worked well in stopping penetrometer insertion upon reaching exceedingly high total resistive forces. Due to the aforementioned suspension issue, the defined cut-off point was set to a higher safety factor to avoid damage to the sensor system during field testing.

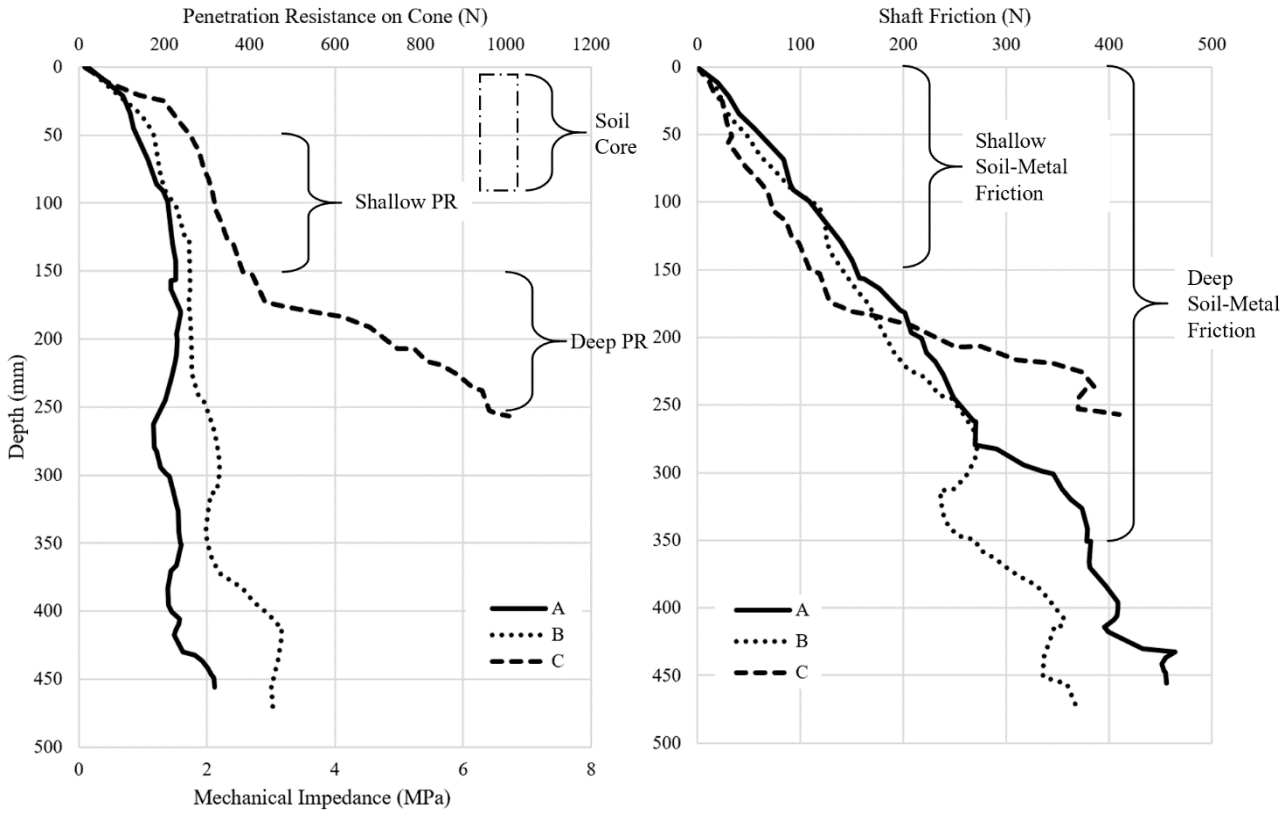

Figure 4.1 Mechanical impedance and shaft friction profiles for 3 locations

Comparisons between the shaft friction profile and cone mechanical impedance profile show that the shaft friction was not entirely separate from the cone impedance, as observed in Figure 4.1. Changes and trends in the impedance profile are reflected in the shaft friction profile, indicating that a certain amount of penetration resistance was transferred to parts of the penetrometer other than the cone tip. This may be a result of internal metal-metal friction between the cone tip/internal rod and the outer shaft. However, given that it is the scale of the friction over depth that is of interest rather than the overall fluctuations, it can be presumed that these fluctuations can be ignored in favor of the general slope; that is, how much friction force acts on the penetrometer as the exposed shaft surface area increases. This measurement becomes more variable as more surface area is introduced; thus deeper penetration results in more informative friction profiles.

4.1.2 RK 520-02

During field testing, the RK520-02 probes and body seemed to withstand repeated insertion. The sensor cable insulation was constructed of soft rubber that could have benefited from more protection. There was signification variation in the measurements within the field, specifically for the VWC measurement, as visualised in Figure 4.2. The temperature measurements were more closely grouped, with large differences being attributed to the warming of the soil as the day progressed. The electrical conductivity measurements were generally lower than desired for agricultural purposes with a mean of 102.6 mS/m and a population standard deviation of 70.2 mS/m.

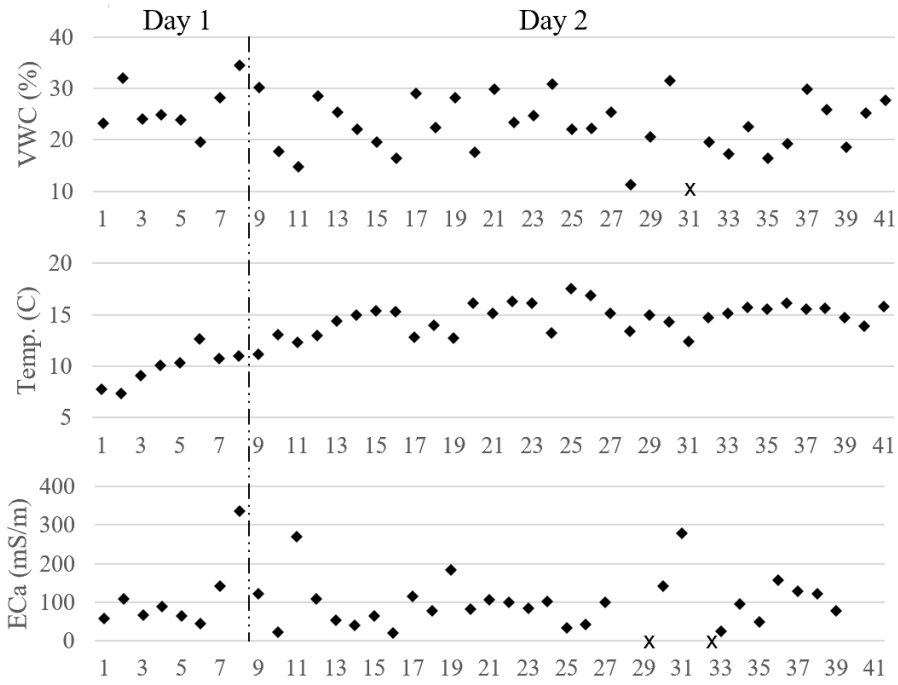

Figure 4.2 Distribution of RK520-02 sensor values over Dataset 2

4.1.3 Air Permeameter and CO_2

The CO_2 sensor design requires cycling of the air between measurements in order to flush the sensor with ambient air and return to an atmospheric baseline. For the initial testing on the Gator vehicle, values fluctuated wildly without inserting the probe, indicating the sensor was likely affected by CO_2 present in

the exhaust fumes. The sensor system was designed for an electric vehicle and thus, exhaust interference was not considered when designing the CO_2 sensor. The sensor began each measurement with a period of values very different than the rest of the experiment. Some of these values created peaks up to 9000 ppm (possibly a result of exhaust fumes during cycling). The sensor has a delayed response in updating its concentration value after the sample extraction as observed in Figure 4.3, likely an artifact of the fouling of the sensor membrane and its effect on the ability of the sensor to respond to changes in concentrations. Though the sensor was washed with clean air from an external air compressor and recalibrated, the issues remained. It is possible that the contamination of the CO_2 sensor has lasting effects in that exposure to high concentrations significantly impact the sensor's ability to measure lower concentrations due to membrane fouling. The CO_2 concentrations, as a result of exhaust interference and sensor membrane damage, were not considered for analysis.

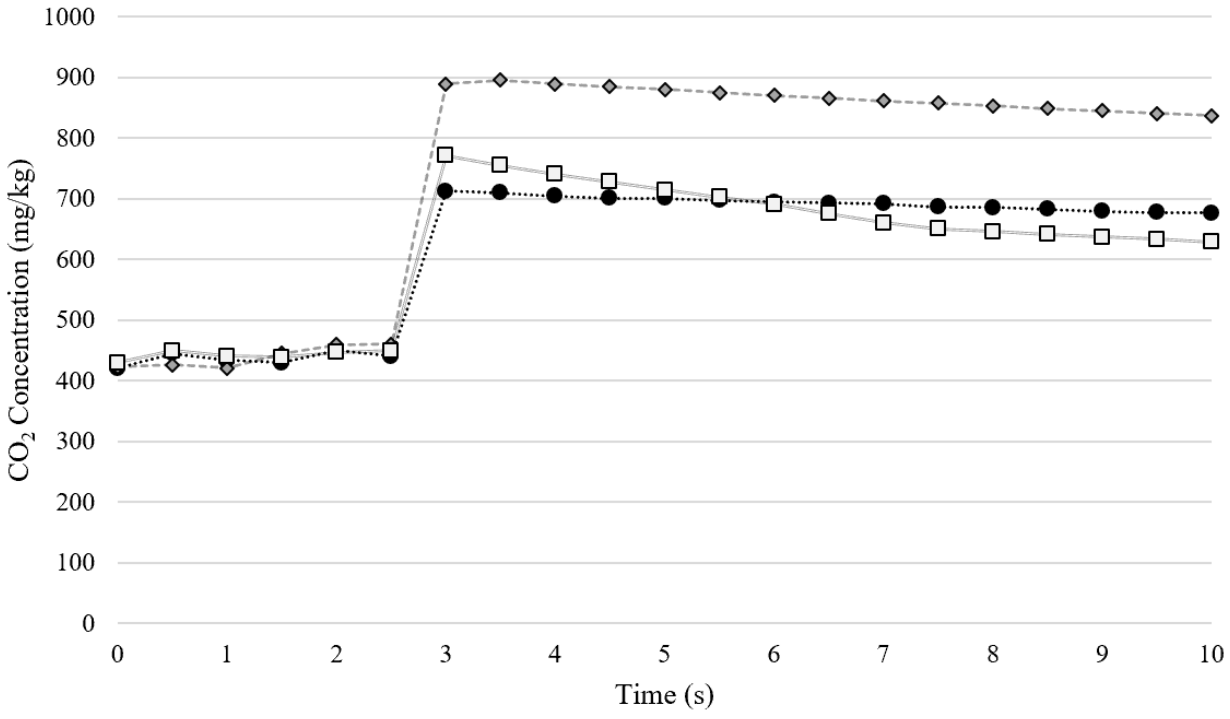

Figure 4.3 CO_2 Concentration over 10-second duration of 4 measurements from Dataset 2

The air permeameter measured resulting air pressure due to injection as designed. In contrast to the previous literature on soil air permeameters, this project's design injected air from below the soil rather than from above, presenting additional factors for consideration such as the possibility of air travelling through

fractures in the soil structure caused by the insertion of the probe rather than through the pore space. The permeameter worked reliably, with the cycling of air at the end ensuring all 16 holes remained clear of soil when inspected between measurements. Prior to entering the field, any dried soil from previous testing was removed. The pressures recorded ranged from 10 to 65 kPa, exhibiting profiles as seen in Figure 4.5. Figure 4.4 shows that the difference between the averages of the first second and middle two seconds is functionally the same with an R^2 of 0.97, with the average between 1-2 seconds slightly higher on average as a result of those initial peaks. As a result of these varying curves to steady state within the air permeameter, the ratio between the average pressure for the 1st second of injection (1-2 seconds of measurement period) and the average air pressure between 2 and 4 seconds was considered and is illustrated in Figure 4.4. Ratios of less than 1 (above unity line) indicate that the initial pressure was higher than the steady-state pressure, with ratios greater than 1 indicating that there was a rise to the steady-state pressure. This ratio may serve as an indication of the soil texture, with higher initial pressures reflecting susceptibility to air permeation.

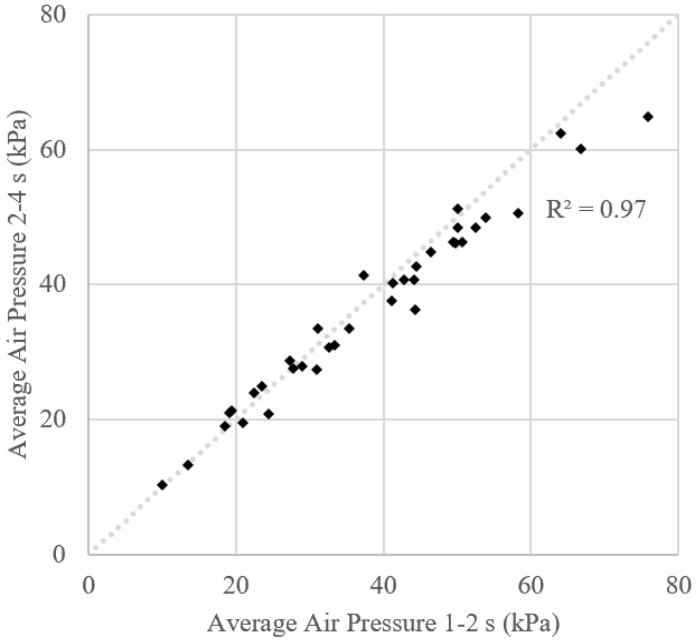

Figure 4.4 Average air pressure over 1-2 s duration vs. 2-4 s duration with unity line

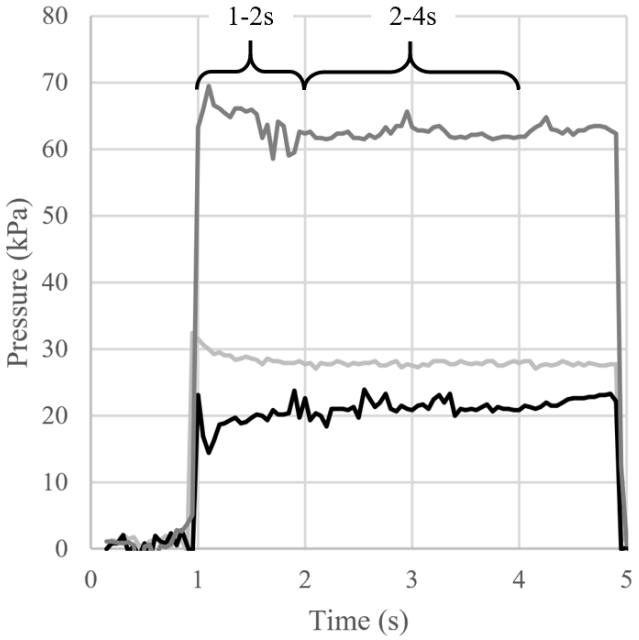

Figure 4.5 Example of 3 air injection pressure measurements over the 5-second measurement period and 4-second injection period

4.2 **Field test 1**

4.2.1 General comparisons

A Pearson correlation matrix was calculated to determine sensor interactions as well as dependencies for all variables in the dataset. The short forms of the variables are presented in Table 4.1 along with their corresponding units. The Pearson correlation matrix for Dataset 1 is presented in Table 4.2.

Table 4.1 Short form of variables in Pearson correlation matrices

Variable Short Form	Variable significance and units
Elevation	*Elevation of the measurement (m)*
Veris EC	*EC_a data interpolated from a Veris Quad EC1000 (dS/m)*
RK520 EC	*EC_a measurement from the RK520-02 (dS/m)*
RK520 VWC	*Volumetric water content measured by RK520-02 (cm^3/cm^3)*
RK520 T	*Temperature measurement from RK520-02 (°C)*
PR Shallow	*Average penetration resistance on cone 50-150mm (MPa)*
PR Deep	*Average penetration resistance on cone 150-250mm (MPa)*
PR Ratio	*Ratio between shallow and deep PR (MPa/MPa)*
SMF Shallow	*Slope of friction over depth up to 150mm (N/cm)*
SMF Deep	*Slope of friction over depth up to 350mm (N/cm)*
SMF Ratio	*Ratio between shallow and deep SMF ((N/cm)/(N/cm))*
AP 1-2	*Average air pressure for first second of injection (kPa)*
AP 2-4	*Average air pressure for middle 2 seconds of injection (kPa)*
AP 1-4	*Average air pressure over first 4 seconds of injection (kPa)*
AP Ratio	*Ratio between AP 1-2 and AP 1-4 (kPa/kPa)*
FS T	*Temperature measurement from FieldScout EC110 (°C)*
FS EC	*EC_a measurement from FieldScout EC110 (dS/m)*
FS VWC	*Volumetric water content measured by FieldScout TDR200 (cm^3/cm^3)*
BD	*Laboratory measured bulk density from soil core (g/cm^3)*
GWC	*Laboratory measured gravimetric water content (g/g)*
VWC	*Laboratory measured volumetric water content (cm^3/cm^3)*

Table 4.2 Pearson correlation matrix for Dataset 1, map comparison

	Elevation	*RK520 EC*	*RK520 VWC*	*RK520 T*	*PR Shallow*	*PR Deep*	*SMF Shallow*	*SMF Deep*	*Air Pressure 1-4*	*Veris EC*
Elevation	1.00									
RK520 EC	-0.23	1.00								
RK520 VWC	0.11	0.27	1.00							
RK520 T	-0.10	0.32	-0.27	1.00						
PR Shallow	0.12	0.07	-0.29	0.17	1.00					
PR Deep	-0.06	-0.07	-0.38	0.20	0.51	1.00				
SMF Shallow	-0.28	0.42	-0.18	0.10	0.36	-0.13	1.00			
SMF Deep	-0.54	0.36	-0.18	-0.20	-0.05	-0.06	0.59	1.00		
Air Pressure 1-4	0.15	0.29	0.48	-0.24	0.21	-0.29	0.10	0.07	1.00	
Veris EC	-0.10	0.62	0.28	-0.13	0.04	-0.10	0.09	0.48	0.48	1.00

The cone penetrometer showed only one clear correlation within the variable set captured in Dataset 1. The penetration resistance on the cone over both the shallow and deep profiles had a slight correlation with the RK520-02 VWC, though the lack of a strong correlation where it might otherwise be expected is likely a result of poor performance by the RK520-02 VWC measurement rather than the cone penetrometer. The RK520-02 VWC showed little correlation with the elevation of the field, even at the lowest elevations where water content is expected to be the highest. Comparing the soil-metal friction, represented by the

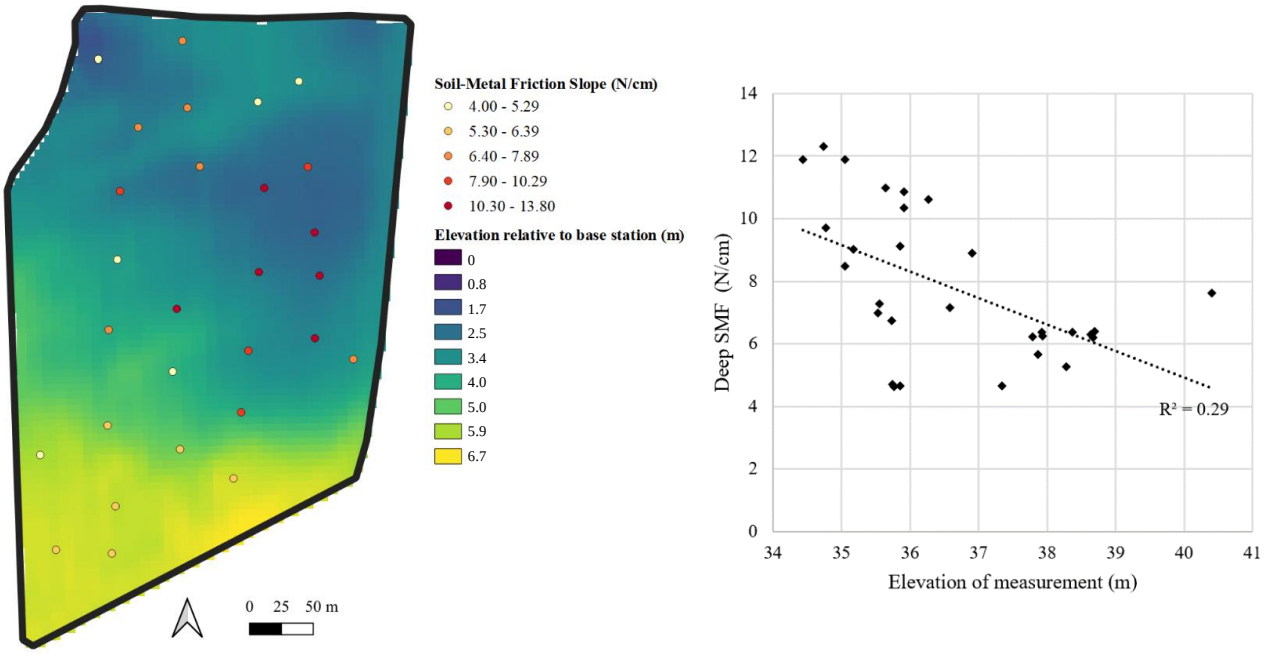

Figure 4.6 Soil-Metal Friction vs. elevation of Dataset 1

friction slope from the cone penetrometer, and the elevation of the test field indicates a general trend in that lower elevations see a larger soil-metal friction as observed in Figure 4.6. For subsequent analysis, an outlier test was run using RStudio 1.3.1913 outlier test (Boston, MA, USA) with three outliers removed. The Pearson correlation coefficient shows a negative interaction at -0.54, and a linear regression yields a p-value of 0.002255 indicating this relationship is statistically significant. This trend might be the result of the higher soil water content found at lower elevations within the field. The east section of the field has more of a ponding effect and poor drainage, while the northwest section of the field is near a drainage ditch and may not have similar soil water content compared to the eastern section as a result of this improved drainage, creating the aforementioned outliers. In general, the lower elevations have a higher soil-metal friction value.

Mapping the RK520-02 data over a high density spatial map of EC_a generated by a Veris Technologies Quad EC1000 (Salina, KS, USA) shows that the RK520-02 is able to capture general trends within a field as seen in Figure 4.7. The zero-intercept linear regression between the RK520-02 and the Veris data is

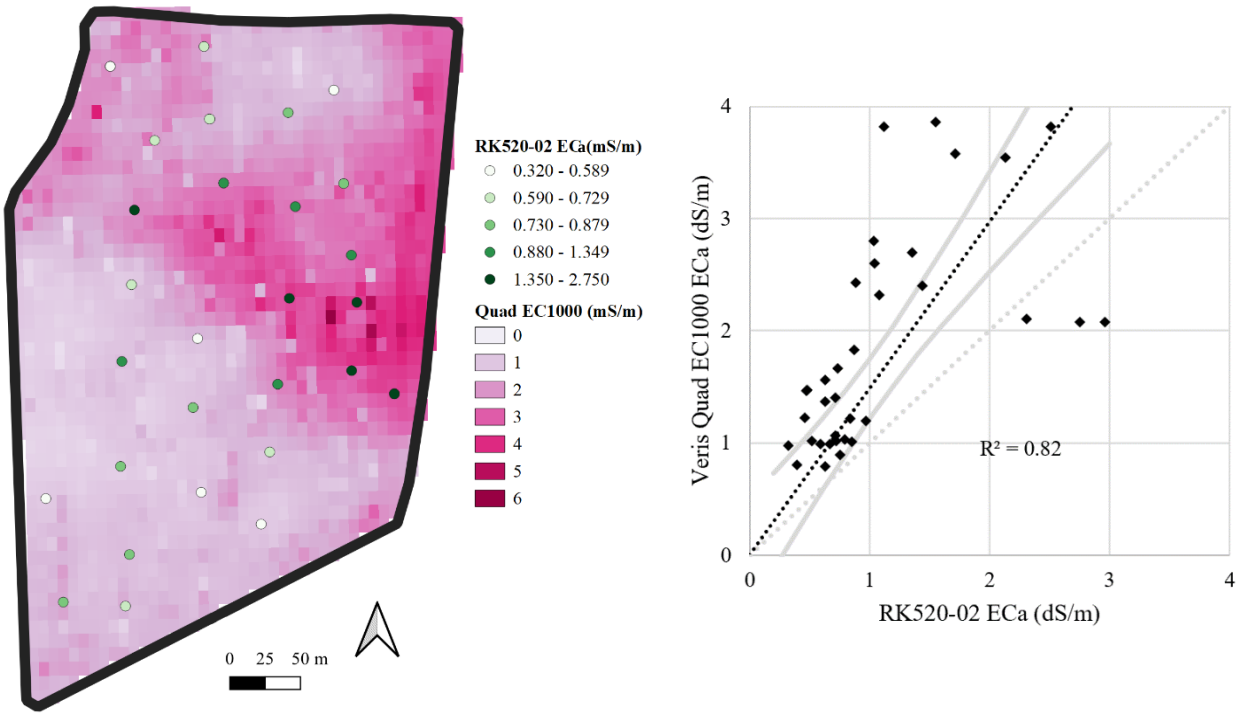

Figure 4.7 RK520-02 EC_a over Veris Quad EC1000 map and linear regression with 95% confidence interval

highly significant with an R^2 of 0.82. Differences in the range of values captured by the two sensor systems may be a result of the time difference between the collection of measurements by the two sensors of approximately one month, as well as calibration differences.

Also of note, but of marginal significance, is the relationship between the RK520-02 VWC and the average air pressure within the 1-4 s interval. This correlation may be due to the relationship between soil water content and intrinsic permeability of the soil, though once again, evaluation of this interaction relies on the accuracy of the VWC measurement.

4.3 **Field test 2**

4.3.1 Pearson Correlations

All variables collected in Dataset 2 are presented in a Pearson correlation matrix as seen in Table 4.3. The data includes all measurements from the sensor system, FieldScout commercial sensor measurements, and the laboratory measurements of water content and bulk density.

Table 4.3 Pearson Correlation matrix for Dataset 2; lab and commercial sensor comparison

	BD	*RK520 VWC*	*RK520 T*	*RK520 EC*	*FS VWC*	*FS T*	*FS EC*	*GWC*	*VWC*	*AP 1-4*	*AP 1-2*	*AP 2-4*	*AP Ratio*	*PR Shallow*	*PR Deep*	*SMF Shallow*	*SMF Deep*	*SMF Ratio*	*PR Ratio*
BD	1.00																		
RK520 VWC	0.15	1.00																	
RK520 T	-0.29	-0.31	1.00																
RK520 EC	-0.04	0.44	-0.24	1.00															
FS VWC	-0.30	0.00	0.52	0.12	1.00														
FS T	-0.35	-0.17	0.72	0.09	0.31	1.00													
FS EC	-0.41	-0.04	0.08	0.37	0.26	0.32	1.00												
GWC	-0.74	0.03	0.33	0.18	0.55	0.41	0.42	1.00											
VWC	0.17	0.25	0.10	0.18	0.41	0.15	0.07	0.52	1.00										
AP 1-4	-0.18	0.38	0.14	0.03	0.35	0.27	0.20	0.27	0.12	1.00									
AP 1-2	-0.18	0.43	0.12	0.07	0.37	0.21	0.25	0.26	0.11	0.99	1.00								
AP 2-4	-0.19	0.37	0.14	0.03	0.35	0.28	0.20	0.28	0.12	1.00	0.99	1.00							
AP Ratio	0.05	0.50	-0.06	0.15	0.26	-0.24	0.23	-0.02	0.04	0.43	0.54	0.40	1.00						
PR Shallow	0.48	-0.18	-0.10	-0.26	-0.35	-0.22	-0.24	-0.59	-0.27	-0.08	-0.09	-0.09	-0.09	1.00					
PR Deep	0.46	-0.17	-0.39	-0.20	-0.45	-0.35	-0.25	-0.51	-0.12	-0.30	-0.30	-0.31	-0.12	0.67	1.00				
SMF Shallow	-0.08	-0.08	0.56	-0.12	0.26	0.34	0.23	0.20	0.14	0.48	0.46	0.49	-0.01	0.27	-0.37	1.00			
SMF Deep	-0.34	0.08	-0.02	0.20	0.06	0.22	0.58	0.34	0.01	0.58	0.58	0.58	0.13	0.16	0.20	0.34	1.00		
SMF Ratio	0.28	-0.18	0.37	-0.41	0.20	-0.02	-0.46	-0.11	0.21	-0.28	-0.28	-0.28	-0.03	0.13	-0.17	0.31	-0.70	1.00	
PR Ratio	-0.26	0.09	0.38	-0.01	0.35	0.31	0.18	0.30	0.07	0.31	0.30	0.31	0.04	0.20	-0.51	0.72	0.19	0.20	1.00

4.3.2 Cone Penetrometer

The profiles generated by the DLCP and the handheld Field Scout SC900 appear to follow similar trends through the soil profile, though the profile of the SC900 appears to be scaled down in both depth and force. The Field Scout SC900 uses an ultrasonic sensor to determine penetration depth, and this can be impacted by crop reside on the surface, which sometimes results in a distorted profile in which the recorded depth is not accurate leading to a distorted reflection of the soil profile. Additionally, the processor used by the SC900 appears to be rather basic, recording values only every 25 mm. Over a multitude of measurements, a noticeable trend appears in which force values are repeated, either due to rounding or limitations of the onboard processor. The DLCP provides a higher resolution compaction profile of the soil and eliminates all the operator-induced errors that occur with the FieldScout unit, mainly, the variations in speed, force, and angle during and between individual measurements. Figure 4.8 shows a comparison of profiles between the two units, with Figure 4.10 showing the general variation between the two sensors, notably the larger penetrometer values recorded by the DLCP. This variation in scale is likely a result of improper calibration between the two sensors.

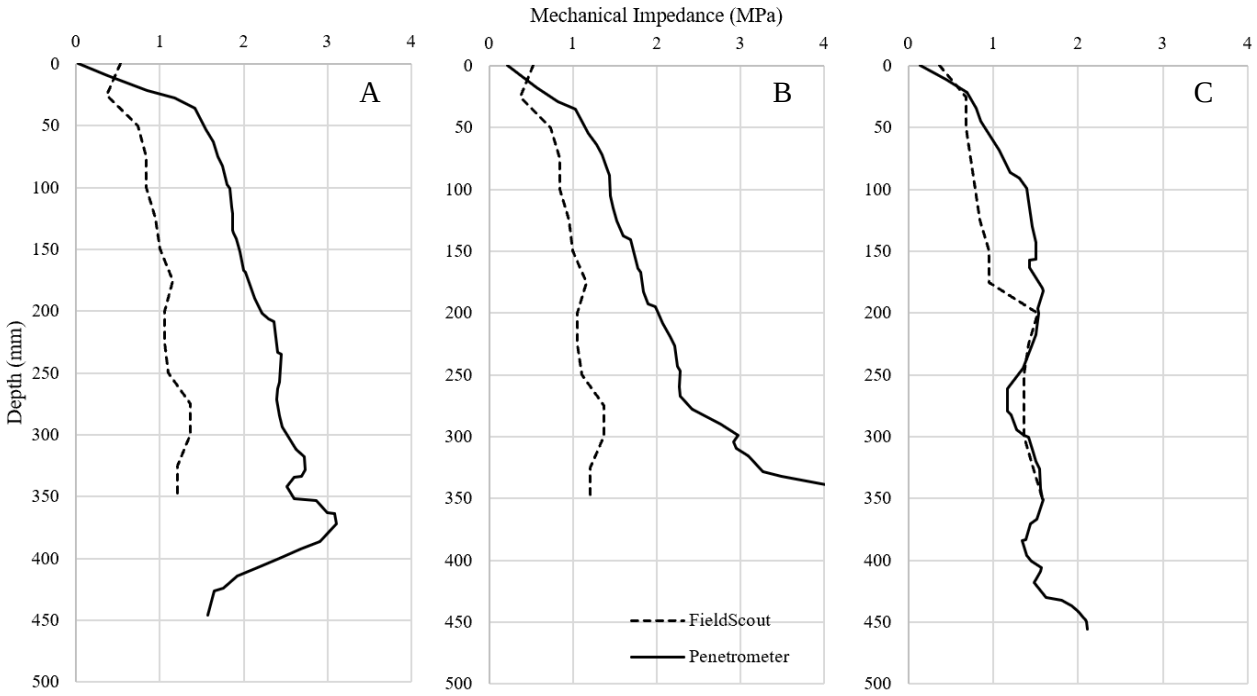

Figure 4.8 Three comparisons between DLCP vs. FieldScout SC900 penetration resistance profile

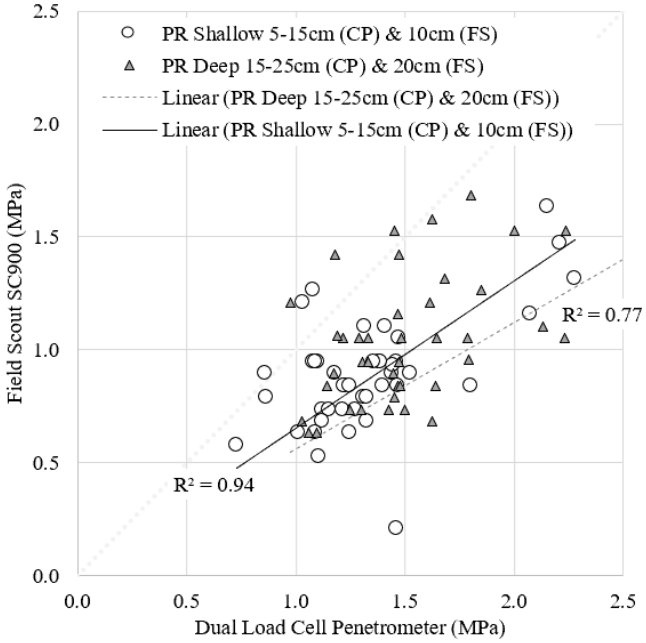

Figure 4.10 FieldScout SC900 vs. DLCP for shallow and deep penetration resistance values

For the penetration profile, averages and maximum values between the various depths were considered. For the friction profile, the slope was considered from 0 to depths of 150 mm and 350 mm. The first 50 mm of each reading was not considered for penetration resistance due to possible aberrations resulting from root matter. The average value between 50-150 mm was chosen for analysis as a shallow value, with 150-

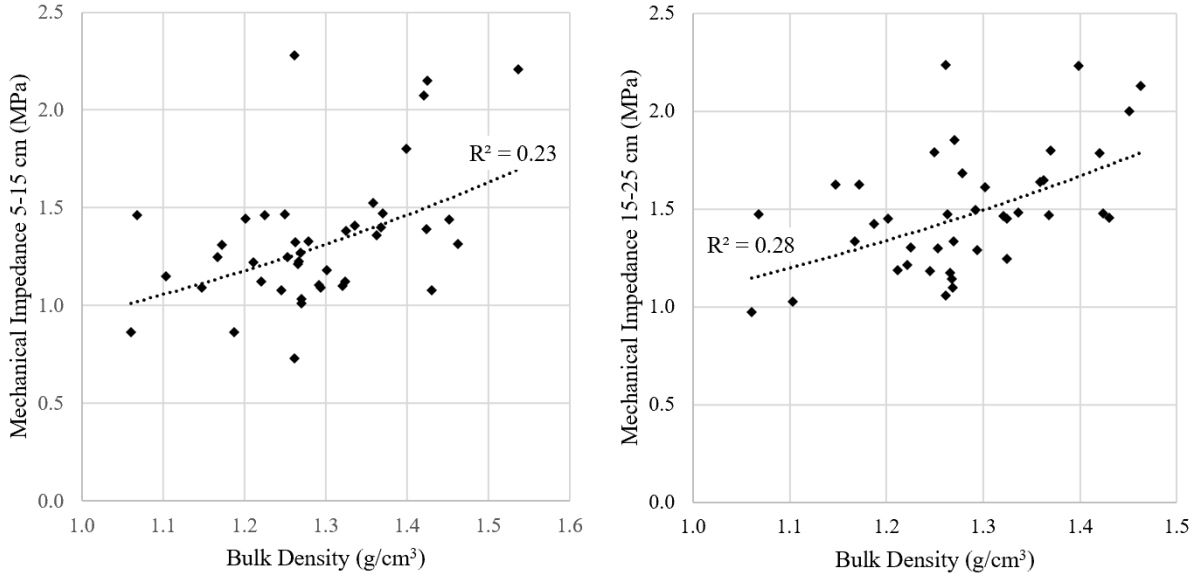

Figure 4.9 Penetration resistance shallow (5-15 cm) (left) and deep (15-25cm) (right) vs. bulk density

250 mm as a deep value. Figure 4.9 exhibits the relative similarity between the two depth ranges in relation to bulk density, with an exponential function selected based on Vaz et al. (2011) relation equations between PR, BD, and water content, to demonstrate the correlation. A simple linear regression of shallow PR to BD yields a similar R^2 of 0.23, with a p-value of 0.001, whereas the simple linear regression of deep PR to BD yields a p-value of 0.002. As the bulk density relates to the soil core taken from the top 100 mm of soil, the shallow measurement should be a more accurate reflection of bulk density; however, the field in which these measurements were taken is well managed and thus there may not be significant variations between compaction of the topsoil and subsoil layers. The slightly lower R^2 between the shallow PR and BD in the exponential model may be a result of incorporated crop residue leading to more variation in PR.

The deep penetration resistance exhibits a tighter correlation to the gravimetric water content as seen in Figure 4.11 using exponential correlation equations as recommended by Vaz et al. (2011). This improved correlation compared to the shallow penetration resistance may be the result of fewer additional factors impacting the penetration resistance. The deeper soil layer may offer a penetration resistance that is more representative of overall soil bulk density and water content. Generally, however, the trends exhibited by both shallow and deep penetration resistance with the gravimetric water content is comparable. There is

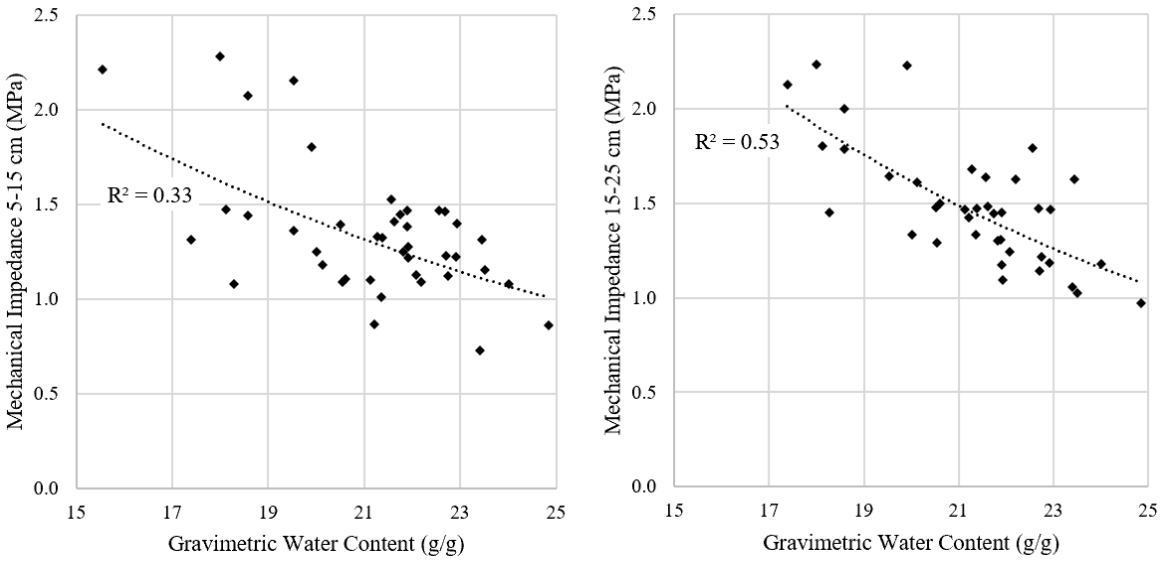

Figure 4.11 Penetration resistance (15-25 cm) (left) and deep (15-25 cm) (right) vs. gravimetric water content

more significant Pearson correlation with the laboratory gravimetric water content than the volumetric water content (-0.59 vs. -0.29), which may be the result of the soil's water retention abilities.

As observed in Figure 4.12, the soil-metal friction generally increases with increased gravimetric water content, as expected due to the increased adhesion with a statistically significant p-value of 0.03. An inverse effect is seen between the soil-metal friction and bulk density, which may be due to the increased water contents found in soils with lower bulk density, however the linear regression relationship is also statistically significant with a p-value of 0.03. Taking the soil-metal friction slope from the values between 0-200 mm rather than 0-350 mm results in a slightly higher slope overall, likely a result of force transmitted from the penetration tip to the penetrometer's internal shaft from friction within the tool. Using the friction over 0-350 mm in the analysis provides more data with which to ensure the force considered in the slope calculation comes from the soil-metal friction, rather than potential transmission of penetration resistance through the internals of the penetrometer. The soil-metal friction slopes up to the deeper value were observed to be more representative of the soil-metal friction, likely a result of the increased surface area between soil and penetrometer shaft at greater depths generating an increased effect. As the penetrometer moves through the soil, it is in constant contact with the 20-100 mm topsoil layer from which the soil core used for laboratory analysis of water content and BD was removed. The laboratory measurement of water

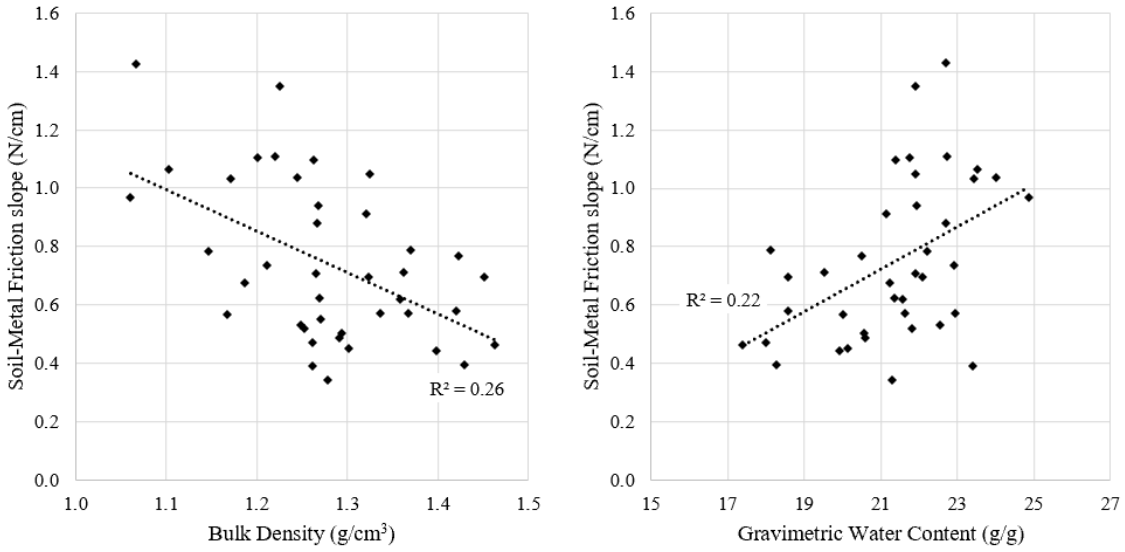

Figure 4.12 Deep soil-metal friction vs. gravimetric water content (left) and bulk density (right) with best fit lines

content and BD from this soil core layer are thus directly affecting the deep soil-metal friction value throughout the stroke of the penetrometer.

4.3.3 RK 520-02

Evaluation of the RK520-02 indicated that of its three measurement parameters, the soil volumetric water content reading was highly questionable. The measured values appeared to vary widely compared to laboratory measurements. Relative to the laboratory measured VWC, there was a considerably wider range of measurements for the RK520-02 with a range of ~11-35% VWC compared to ~22-32%. Comparing the RK520-02 measurement directly to laboratory volumetric water content yields no significant correlation as illustrated in Figure 4.13, with a p-value of 0.13. The FieldScout TDR200 exhibited only a marginally better correlation with the laboratory measurements, however, the relationship was significant with a p-value of 0.0084. Spatial variation would not account for such discrepancy; and thus, it may be a result of incomplete insertion of the probe or poor sensor reliability.

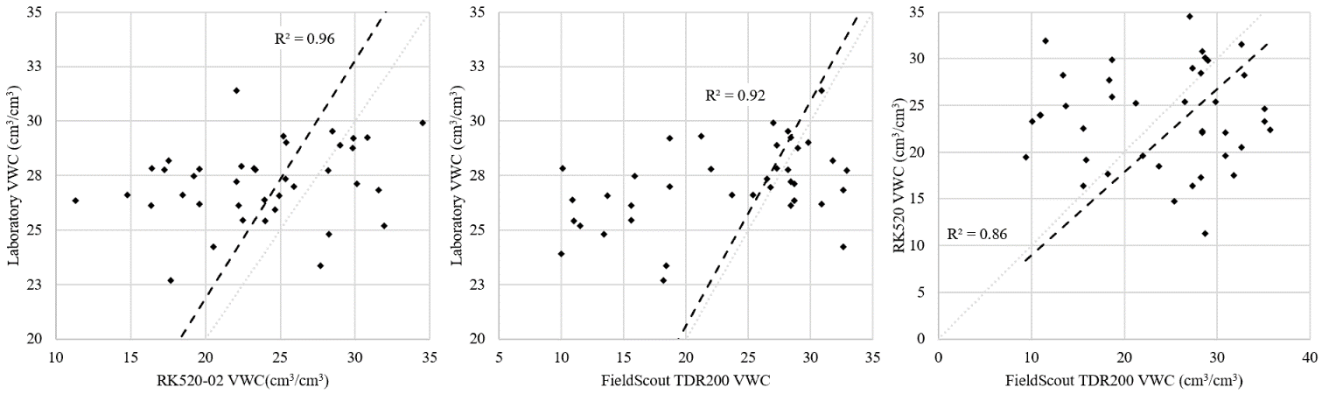

Figure 4.13 Zero-intercept regressions between RK520-02 VWC, FieldScout TDR200, and Laboratory measured VWC

While a laboratory analysis of soil EC_a for each measured location is required to determine the accuracy at which the RK520-02 determines EC_a, comparison to conventional handheld units shows undesirable variation. The RK520-02 appears to underestimate values. Compared to the handheld EC110, the R^2 is 0.70 with a zero intercept, as seen in Figure 4.14, however the relationship is only just significant with a p-value of 0.025. It is not certain what caused this poor relationship; it could be a result of spatial variation amplified by probe insertion location during measurement, or a reflection of sensor error, requiring further testing to

verify. The two sensors use quite different technologies in EC_a measurement, with the FieldScout using a dipole electrode configuration and the RK520-02 using the FDR principle.

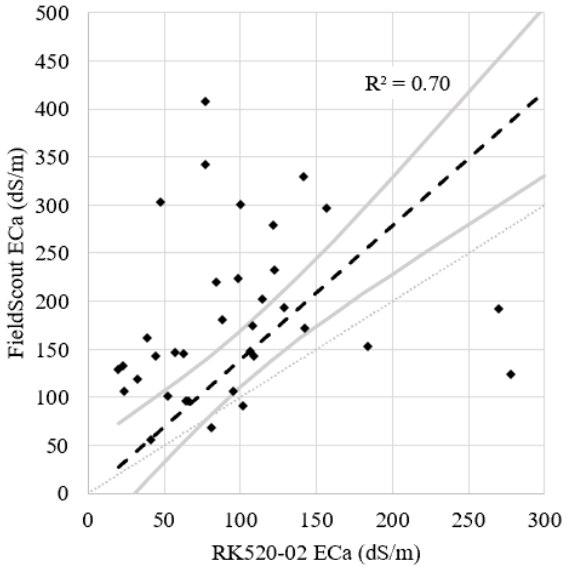

Figure 4.14 RK520-02 EC vs. FieldScout EC110 EC linear regression with 95% confidence interval

The temperature measurement appears to be the only parameter for which the RK520-02 and commercial FieldScout units are highly correlated. As seen in Figure 4.15, this relationship presents an R^2 of 0.98 in a linear regression with zero-intercept and is significant. The relatively high coefficent of correlation may be due to the fact that both instruments use a thermistor to measure temperature.

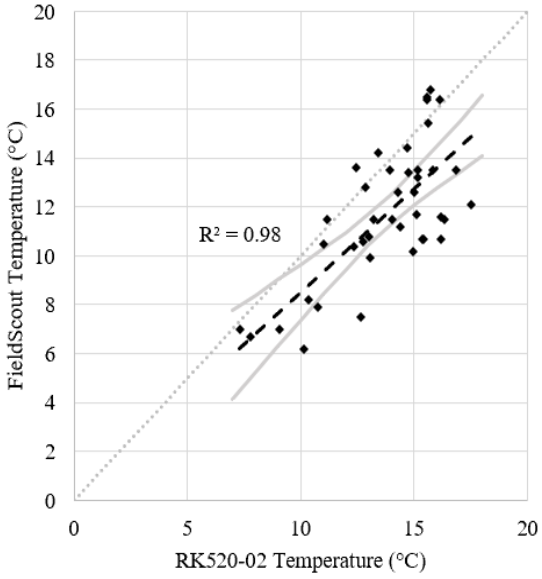

Figure 4.15 RK520-02 Temperature vs. FieldScout EC110 Temperature linear regression with 95% confidence interval

4.3.4 Air Permeameter

An insignificant Pearson correlation of 0.28 was found between the laboratory-measured VWC and the air pressure. The simple linear regression between the average air pressure from 1-4 s and BD was insignificant with a p-value of 0.29. However, though the RK520-02 VWC measurement was of questionable reliability, a higher Pearson correlation of 0.43 was observed between the average air pressure between 1-2 s and RK520-02 VWC, with a general trend that high VWC resulted in a higher average air pressure over the injection period. While this correlation may not necessarily be a result of the soil's actual water content, there may be some soil property that both instruments are responding in a similar way. The dielectric constant of the soil may relate to soil cohesivity, particularly with how clay soils impact the dielectric constant, resulting in the observed correlation between these two measurements. The most significant correlation found in the air pressure measurements was between the air pressure resulting from injection and the soil-metal friction of the cone penetrometer as seen in Figure 4.16, with a p-value of 0.00023. As soil-metal friction increases, so too does the air pressure within the permeameter. This is likely a further result of some combination of soil texture mechanical property and water content and requires further investigation. It should be noted that the air inlet and injection ports are located 150 mm below the soil

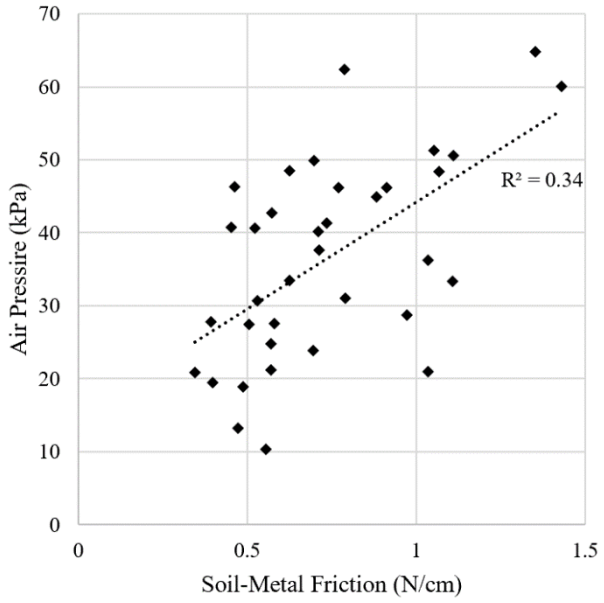

Figure 4.16 Air pressure vs. soil-metal friction

upon air injection, while the spatial area of temperature, EC, and moisture sensor measurements are described by the RK520-02 documentation as being comparable to a 70 mm deep cylinder with a 70 mm diameter centered on the middle probe.

4.4 **Estimation of Bulk Density**

4.4.1 Direct correlations

From the soil cores collected at each measurement point, the bulk density values of each core varied between 1.05 and 1.55 g/cm^3. There was a significant correlation between the gravimetric water content and bulk density, with an R^2 of 0.60 (Figure 4.17). The measurements of permeability, mechanical impedance, and soil-metal friction are presented side-by-side as they relate to bulk density in Figure 4.18. These measurements are affected by physical properties such as soil texture and structure as they relate to porosity, permeability, cohesivity, adhesivity and aggregate arrangement. These measurements of the physical properties of the soil should allow for *in situ* estimation of bulk density.

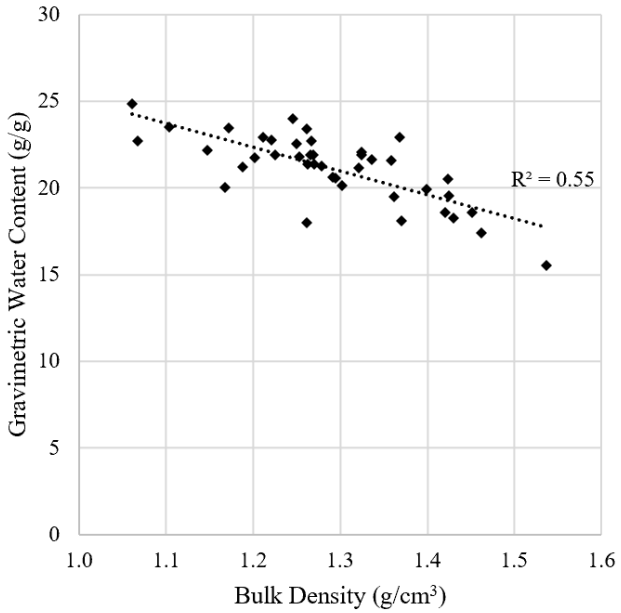

Figure 4.17 Gravimetric water content vs. bulk density of soil cores

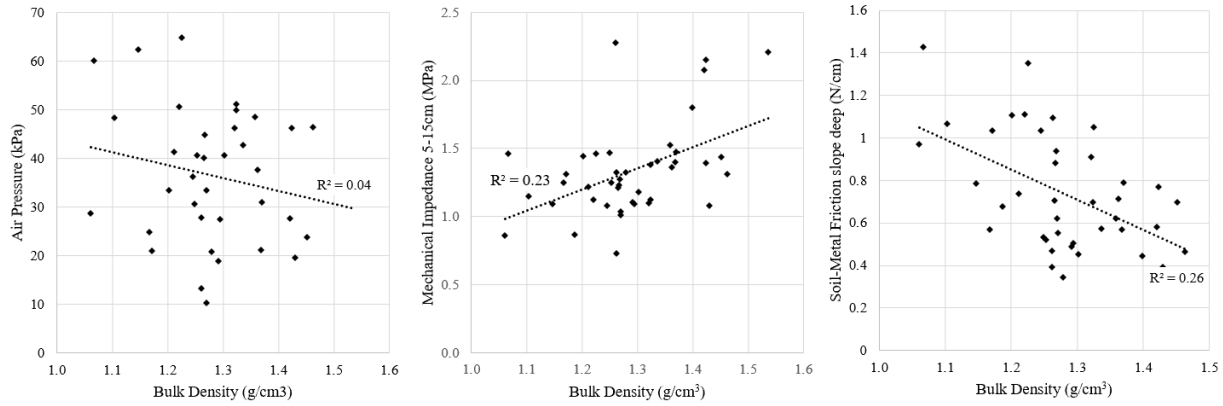

Figure 4.18 Values measuring mechanical properties vs. bulk density

4.4.2 Regression model

To assess the capability of the sensor system to estimate bulk density, a multivariate regression model was derived from the sensor system variables. The resulting best model is presented in the first row of Table 4.4. In consideration of the unreliability of the RK520-02 water content measurement, it can be substituted with the laboratory gravimetric water content to simulate how the model might be improved with a better sensor for soil water content, with the best model using this laboratory value detailed in the second row of Table 4.4.

Table 4.4 Models for estimation of bulk density with sensor system, with laboratory GWC model in bold

Model	Adjusted R^2	RMSE (g/cm^3)
Bulk Density *= RK520VWC + AP14 + AP14² + PRShallow + SMFRatio + SMFDeep + PRRatio + RK520VWC*SMFDeep + RK520VWC*SMFRatio + RK520VWC*PRShallow*	0.57	0.0636
Bulk Density *= RK520EC + SMFDeep + SMFDeep**__Laboratory GWC__* *+ SMFRatio + PRRatio*	0.57	0.0580

Both models are graphed relative to the actual bulk density in Figure 4.19. When using the model derived from only the sensor system, there is more error; however, over the range of bulk densities captured in this experiment. The model is capable of providing an estimate of bulk density with the slope of the zero-intercept regression, R^2=0.70, not statistically different from 1 with alpha=0.05. Notably, the model for bulk density using only sensor system variables appears to incorporate the interactions one would expect, including the interactions between the RK520-02 VWC with SMF, SMFRatio, and PR. This model is certainly unique to the soil type and moisture conditions of the dataset. If the sensor system is to be used to estimate bulk density, the model must be calibrated over a wide variety of soil types, water content, and compaction levels.

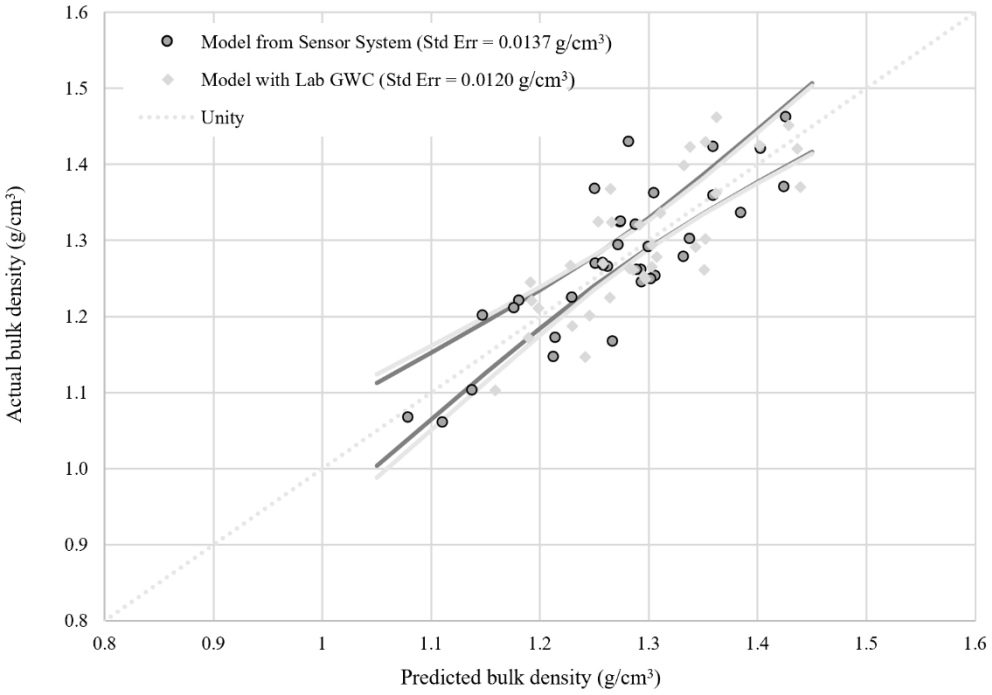

Figure 4.19 Model predicted bulk density vs. actual bulk density with 95% confidence interval of regression fit

4.5 **Discussion**

Overall, the capability of the sensor to perform autonomous measurements proved to work as intended and withstand the forces of insertion. There are several areas of the system that could be improved; however, when the system is eventually paired with the Bearcub 24, most of these issues would be resolved. These problems include the cone penetrometer force lifting of the measurement vehicle, declining voltage from

the lead-acid battery over the course of a day, and the susceptibility of the CO_2 sensor to exhaust fumes. The solid construction of the Bearcub 24 will provide a stable platform for the penetrometer to ensure that no lifting of the sensor system occurs. The improved batteries of the Bearcub 24 provide a more stable voltage and current which help to maintain the speed and force with which the penetrometer enters the soil, and the electric motor does to not produce exhaust that could contaminate soils.

Prior literature indicates that the parameters measured by the cone penetrometer and air permeameter are highly dependent on the volumetric water content of the soil. Unfortunately, given the results of this experiment, the RK520-02 does not present usable VWC data in this configuration. The lack of correlation between the RK520-02 VWC and both lab and FieldScout values suggests that while the spatial variation resulting from the distance between probes may play a part, the principal difference is the result of poor sensor performance. When building the model to estimate bulk density, substituting the laboratory value for water content resulted in a slightly improved model. This suggests that the principal failure of this design is in the measurement of water content. Even the FieldScout TDR unit performed only marginally better than the RK520-02 compared to laboratory values, suggesting that more work is needed in the selection of a suitable VWC sensor for this sensor system. Documentation of the RK520-02 lists the accuracy of the sensor as ±2%, which may account for some of the variation (Rika Corp, 2021). FDR sensor accuracy can be improved with calibration specific to the soil-type (Ojo et al., 2015). Given the autonomous nature of the use, future research would benefit from the selection of a water content sensor that is accurate in a wide variety of situations without requiring frequent calibration. Prior literature was able to use only PR and VWC to estimate bulk density (Vaz et al., 2011). The EC_a component of the RK520-02 appears to be capable of capturing at least the general trend of a field, despite showing little correlation with its handheld counterpart, the FieldScout. The slightly higher temperatures recorded by the RK520-02 versus the FieldScout may also be a result of improper calibration of either sensor.

The lack of reliable field VWC measurements impacts most other sensor measurements, as their parameters are dependent on soil VWC. The PR of the cone tip at 50-150 mm correlated well with the laboratory VWC,

with lower water content indicating that the soil is dense, leaving less pore space for water. Dryer soils will also exhibit a higher mechanical impedance as a result of their more rigid soil structure at low water content, highlighting the reasons why accurate VWC measurements are needed to correct the PR measurement in determining soil bulk density. The PR values were closely grouped, with few measurements exceeding 2 MPa; however, the majority of bulk density values were also on the lower end, grouped between 1-1.5 g/cm^3, whereas it is only above 1.6 g/cm^3 that root growth is restricted, with extremely high compaction presenting BD of up to 2 g/cm^3 (Brown & Wherett, 2021) This lack of variation is a result of the test fields being well maintained, tilled, and thus, relatively homogenous. Greater variety of bulk densities and compaction levels would help to provide a better evaluation of the efficacy of the cone penetrometer in determining bulk density through its penetration resistance measurement. Additionally, the load cells used in the penetrometer were deployed with the factory calibration curves, rather than calibrated on-site. This may explain why the DLCP exhibited consistently higher values than the FieldScout SC900. Alternatively, the FieldScout SC900 had not been calibrated for an extended period; thus, the discrepancies may be a result of both penetrometers lacking adequate calibration. Nevertheless, the DLCP uses a much more reliable method of measuring the depth of measurements through its reference potentiometer in the linear actuator, though the value of high-resolution depth profiles compared to the average between specified depths depends on what information is needed from the penetrometer. Further analysis into the differing PR values in different soil layers may reveal some benefit in both locating the depth of the hard pan, as well as better characterization of the topsoil health.

With regards to the soil-metal friction, a distinct correlation was observed with the GWC. The resulting linear regression shows promise, but it is not the expected behaviour of this relationship. At higher ends of GWC, it is expected that the soil-metal friction would decrease as the soil water starts acting more as a lubricant and less as a binder for the soil particles. This was not observed from either dataset; nevertheless, there was little variation in gravimetric water content, with minimum and maximum values of only 16% and 25%, respectively. The dataset may show the adhesion increase up to 25% moisture content, insufficient

to reach the lubrication range for the soil texture of the tested field. Further research should include a greater range of soil water content over the same soil texture. The variation in soil-metal friction is also highly dependent on soil texture, with more clay soils exhibiting greater elasticity. An explanation for the decrease in soil-metal friction as bulk density increases may be the result of the reduced adhesion effect. In soils with higher bulk densities, there are less pore spaces for water to occupy and thus, contribute to an adhesive effect on the penetrometer shaft. Additionally, soils with higher bulk densities will exhibit tighter soil particle arrangements, and once displaced by the initial cone, will remain in their new configuration rather than applying force back on the penetrometer shaft when returning to its original position, as wet soil might. This soil-metal friction value may be of use to farmers such that they can determine areas of the field where they may encounter more soil-tool friction during plowing or tillage operations. This may also be used as another indicator of soil-water capacity, where soil-metal friction and water content exhibit a relationship connected to the soil's water retention capabilities.

The design of the air permeameter appears to respond to different soil types, though more laboratory analysis of the soil cores would be needed to determine how soil texture correlates with the permeability and water content measurements. As the air is injected into the soil, any initial spike in pressure results from cavitation from the high pressure air through the probe outlet holes. The pressure that follows represents the soil macropore size and connectivity, with larger pores allowing greater air flow and a lower pressure reading. Soils with a lower percentage of macropores would restrict air flow, increasing the pressure buildup between the soil and probe interior. As such, the air permeameter measurements represent a component of the soil structure. Higher readings indicate lower pore spaces within the soil structure which may indicate a higher bulk density, though no correlation was observed in this study. This may be a result of the sensitivity of permeameters to the structural differences of different soil types. Beyond soil structure, the air permeameter is likely measuring the soil particle cohesion as well, which would account for the correlation with the soil-metal friction. Higher air pressure values are likely a result of a more cohesive soil and its resistance to injection. With more cohesion between particles, such as seen in clay-textured soils,

soil particles may require more force to displace and restructure to allow air flow when exposed to air pressure whereas a sandier soil would see particles easily displaced by the injected air. The ratio between the initial pressure and steady-state pressure may also be the effect of the cohesive properties of the soil texture. As observed in the literature, soil cohesion is highly dependent on water content, thus any conclusions drawn from the measurements must correct for, or consider, this.

The soil CO_2 sensor shows promise in that initial testing showed it has the capability to extract a certain amount of soil vapour and measure the resulting concentration. Unfortunately, the issue with the diesel vehicle exhaust contaminating the sensor during air cycling made the CO_2 dataset unreliable. As a working principle, the CO_2 sensor design does not account for vertical variability of concentration throughout the soil profile. While it compensated for this by routinely extracting a constant volume of soil gas, there is no correction to determine if the vacuum is primarily pulling macropores above or below the probe inlets. More research is needed to evaluate the efficacy of this sensor design, including testing on an electrical vehicle and comparing the results to laboratory analysis of soil CO_2.

4.6 **Future Improvements**

4.6.1 Design and software improvements

There are a variety of improvements that can be made to this sensor system, beyond the previously discussed replacement of the VWC sensor. As seen in Figure 4.20, updates to the frame could significantly decrease the weight of the sensor system, as well as helping to bring the sensor probes closer together around the central cone penetrometer. Faster linear actuators could allow for faster measurements. Higher quality wire with shielding would help to reduce noise in measurements, as well as crosstalk between sensor wires and the higher current and voltages in the actuator power wires. The cone penetrometer could be improved by substituting the commercially available 60° cone for the standard 30° cone. As Voorhees et al. (1975) found, primary root elongation was more closely correlated with a cone with a smaller vertex compared to a 60°

vertex. Additionally, substituting the internal reference potentiometer for an accurate displacement sensor would allow for proper PID control of the penetrometer speed across a variety of soil compaction levels.

The air permeameter soil-probe seal should be redesigned such that it enters the soil in a ring at the top of the probe, creating a tight seal that ensures no air escapes along the probe shaft to above-ground, impacting the pressure reading. Addition of a flow meter to the permeameter injection port could be an additional metric with which to quantify the soil air permeability, allowing the pressure measurement to be paired with a corresponding flow value.

Figure 4.20 Updated render with streamlined profile, closer probe grouping, and significant material reduction

Beyond these mechanical changes, the integration of the sensor system with the Bearcub 24 will see the control of the system passed onto the Bearcub unit, allowing for additional logic within the code to utilise the Bearcub's onboard optical sensors, more precise control of the sensor system, and processing of data in real time. For example, the Bearcub's optical sensor could ensure the measurement location is not above visibly stony soil or root structures. Additional development of the data analysis portion of the system could make use of the Bearcub 24's connection to a remote server in which machine learning could be used to

optimise the bulk density estimation model relative to the geographical area and further relate measurements to historical records such as yield and soil nutrient data. With the onboard processor, analysis of the measured properties could take place in real time, and logic could be programmed to allow for multiple measurements if an outlier is detected in order to verify the measurement. The sensor system detailed in this paper could be used interchangeably with systems such as that developed by Buelvas et al. (2020), which features 360° Vis-NIR spectroscopy measurements over 0 to 200 mm, onboard automated platforms such as the Bearcub 24.

4.6.2 Extended Field Testing

Extended field testing will allow for better characterization of the sensor system performance with regards to bulk density estimations. Measurements should be made over a great range of soil types within a shorter period to eliminate temporal variation and provide a wider range of soil characteristics for which the system can measure. Multiple soil cores per measurement would help to account for variation induced by subsurface crop residue and spatial variation. Proper calibration of both sensor system sensors and commercial sensors will ensure that comparisons are made relative to standardized values. Additional laboratory analysis of soil cores to include soil texture, EC, and porosity would help to quantify how each sensor within the system is affected by these parameters and their influence on bulk density.

Improved estimation of bulk density should allow for better selection of the number, size, and specification of equipment used in land work to reduce damage to soil structure (Alexandrou & Earl, 1998). Estimation of bulk density could be improved through the addition of a sensor to measure organic C content, as Heuscher et al. (2005) found that organic C content was the strongest contributor to bulk density prediction.

5. SUMMARY AND CONCLUSIONS

The sensor system was effective at measuring physical soil characteristics in an autonomous manner through the insertion of probes. The mechanical functions and autonomous control worked as intended and should interface seamlessly with the Bearcub 24 to provide real-time feedback to the remote operator when developed commercially.

Overall, the datasets used in this paper lacked sufficient variability of soil conditions to form any novel correlations with confidence. Given that the fields used for testing were well managed and did not present any unfavorable soil conditions, relating the measured soil properties to differing soil conditions was not possible. Additional field testing in the future should include a wider range of soil types, water contents, and bulk densities. Future research could include further laboratory assessment of soil mechanical properties including cohesion, adhesion, modulus of elasticity, and porosity. With additional testing and creation of models based on laboratory measured parameters, the sensor system should be able to reliably provide an overview of soil health, as a function of microbial activity, EC_a, texture, and structure. Of the sensors within the sensor system, the cone penetrometer design provided the most detailed dataset and, when compared to commercial alternatives, demonstrated that it was an effective penetrometer platform for the generation of soil penetration profiles. The lack of definitive volumetric water content data due to poor performance by the RK520-02 meant that correcting the penetration resistance (PR) and soil-metal friction (SMF) values for moisture would not be possible using the sensor system alone. Nevertheless, the PR and SMF data exhibited distinct correlations with bulk density and laboratory volumetric water content, allowing for the creation of a model for the sensor system to estimate bulk density.

The air permeameter and CO_2 sensor show promise, but further research is needed to determine their efficacy. Namely, laboratory soil texture, porosity, and water content data would help to relate how well the permeameter's performance correlates with these properties, and how they might be derived from the air permeability measurement from this sensor. Direct reference measurements of CO_2 respiration and soil

porosity would be useful to compare to evaluate the sensor's capability of detecting subsurface CO_2 concentrations. Additionally, efforts should be made to calibrate the permeameter values with respect to the percent macroscopic pore space of the soil samples.

Further tests on the Bearcub 24 platform should eliminate the issues caused by mounting the sensor system on a light suspension vehicle. The Bearcub 24 is an excellent platform for proximal soil sensing, since it is lightweight and mobile, while the lack of internal combustion engine means that such sensitive measurements as soil CO_2 can be made unaffected by fumes from combustion engines. The development of an autonomous sensor system coupled with an autonomous electric tractor has the potential to allow for the creation of large spatial datasets of soil physical properties without requiring heavy soil-compacting machinery or human labour. In turn, this soil physical data should allow for agricultural management decisions that seek to preserve soil health, be it tillage routines or cropping schedules.

6. REFERENCES

Abbaspour-Gilandeh, Y., Hasankhani-Ghavam, F., Shahgoli, G., Shrabian, V. R., & Abbaspour-Gilandeh, M. (2018). Investigation of the Effect of Soil Moisture Content, Contact Surface Material and Soil Texture on Soil Friction and Soil Adhesion Coefficients. *Acta Technologica Agriculturae*. 21(2).

Adamchuk, V., Hummel, J., Morgan, M., & Upadhyaya, S. (2004). On-the-go soil sensors for precision agriculture. *Computers and Electronics in Agriculture*. 44(1), 71-91. doi: 10.1016/j.compag.2004.03.002

Adamchuk, V., Wenjun, J., Rossel, R., Gebbers, R., Tremblay, N. (2018) Proximal Soil and Plant Sensing. *Precision Agriculture Basics,* Chapter 9. https://doi.org/10.2134/precisionagbasics.2016.0093.

Adamchuk, V., Wenjun, J., Rossel, R. V., Gebbers, R., & Tremblay, N. (2019). Proximal Soil and Plant Sensing. *Precision Agriculture Basics* (pp. 123-145). Madison, WI: American Society of Agronomy, Crop Science Society of America, and Soil Science Society of America. 45(2(150)).

AGCO. (2021). Fendt FutureFarm. Fendt. https://www.fendt.com/int/xaver

Alexandrou, A., Earl, R. (1998) The Relationship among the Pre-compaction Stress, Volumetric Water Content and Initial Dry Bulk Density of Soil. *Journal of Agricultural Engineering Research.* 71(1) 75-80, ISSN 0021-8634, https://doi.org/10.1006/jaer.1998.0300.

Archer, J.R., Smith, P.D. (1972). The relation between bulk density, available water capacity, and air capacity of soils. *Journal of Soil Science*. 23(4), 475-480.

ASABE Standards (R2013). S313.3: Soil Cone Penetrometer. ASAE.

Azadegan, B., & Massah, J. (2012). Effect of temperature on adhesion of clay soil to steel. *Cercetari Agronomice in Moldova.* doi: 10.2478/v10298-012-0011-z.

Barrientos, A., Roldán Gómez, J.,Cerro, J., Garzón Ramos, D., García Auñón, P., Garzon, M., & De León Rivas, J. (2018). Robots in Agriculture: State of Art and Practical Experiences. *Service Robots,* Chapter 4. doi: 10.5772/intechopen.69874.

Bengough, A.G., Mullins, C.E., & Wilson, G. (2008). Estimating soil frictional resistance to metal probes and its relevance to the penetration of soil by roots. *European Journal of Soil Science*. 48(4).

Birch, R. Ekwue, E., Phillip, C., Campus, A., & Indies, W. (2016). Soil-Metal Sliding Resistance Forces of Some

Trinidadian Soils at High Water Contents. *The West Indian Journal of Engineering*. 38(2), 52-58.

Blake, G. R. (1965) Bulk Density. *Methods of Soil Analysis: Part 1 Physical and Mineralogical Properties, Including Statistics of Measurement and Sampling, 9.1.* https://doi.org/10.2134/agronmonogr9.1.c30

Brown, K. & Wherrett, A. (2021) Bulk Density – Measuring. *Soilquality.org.au.* Retrieved from *http://soilquality.org.au/factsheets/bulk-density-measurement.*

Buelvas, R. M., Adamchuk, V., De Leener, B., & Mangeat, G. (2020). Development of a Semi-Automated In-Situ Soil Sensor using Vis-NIR spectroscopy. 2020 ASABE Annual International Virtual Meeting 2000052.(doi:10.13031/aim.202000052)

Chen, X., Van Den Broecke, J.W., Liu, G., & Hong, G. (2019). A study on the clay adhesion factor. *Dredging Summit & Expo '19 Proceedings*. Chicago, Illinois, USA.

Cheng, G., He, Y.-N., Yue, T.-X., Wang, J., & Zhang, Z.-W. (2014). Effects of Climatic Conditions and Soil Properties on Cabernet Sauvignon Berry Growth and Anthocyanin Profiles. *Molecules.* 19. 13683-13703. doi:10.3390/molecules190913683.

Chief, K., Ferré, T. P. A., & Nijssen, B. (2006). Field Testing of a Soil Corer Air Permeameter (SCAP) in Desert Soils. *Vadose Zone Journal*. 5(4). https://doi.org/10.2136/vzj2006.0063

Emdad, M.R., Raine, S.R., & Smith, R.J. (2004). Effect of water quality on soil structure and infiltration under furrow irrigation. *Irrig Sci*. 23, 55–60. https://doi.org/10.1007/s00271-004-0093-y

Emmi, L., Gonzalez-de-Soto, M., Parajes, G., Gonzales-de-Santos, P. (2014) New Trends in Robotics for Agriculture: Integration and Assessment of a Real Fleet of Robots. *The Scientific World* 2014.

Fish, A. N., & Koppi, A.J. (2006). The use of a simple field air permeameter as a rapid indicator of functional pore space. *Geoderma*. 63(3-4), 255-264. 10.1016/0016-7061(94)90067-1

Flechard, C. R., Neftel, A., Jocher, M., Ammann, C., Leifeld, J., & Fuhrer, J. (2007). Temporal changes in soil pore space CO2 concentration and storage under permanent grassland. *Agricultural and Forest Meteorology*. 142(1), 66-84. https://doi.org/10.1016/j.agrformet.2006.11.006.

Gebbers, R. (2014). Current Crop and Soil Sensors for Precision Agriculture. *Congresso Brasileiro de Agricultura de Precisao*. Sao Pedro, Brazil.

Halcro, G., Corstanje, Ron & Mouazen, Abdul. (2013). Site-specific land management of cereal crops based on

management zone delineation by proximal soil sensing. *The 9th European Conference on Precision Agriculture,* ECPA 2013. 475-482.

Hashimoto, S., & Komatsu, H. (2006). Relationships between soil CO_2 concentration and CO_2 production, temperature, water content, and gas diffusivity: implications for field studies through sensitivity analyses. *Journal of Forest Research.* 11(1), 41-50. https://doi.org/10.1007/s10310-005-0185-4

Heuscher, S.A., Brandt, C.C., Jardine, P.M. (2005). Using Soil Physical and Chemical Properties to Estimate Bulk Density. *Soil Science Society of America Journal,* 69(1), 51-56, https://doi.org/10.2136/sssaj2005.0051a.

Iqbal, J., Xu, R., Halloran, H., Li, C. (2020). Development of a Multi-Purpose Autonomous Differential Drive Mobile Robot for Plant Phenotyping and Soil Sensing. *Electronics.* 9(9), 1550, https://doi.org/10.3390/electronics9091550.

Iversen, B. V., Schjønning, P., Poulsen, T. G., & Moldrup, P. (2001) *In situ*, on-site and laboratory measurements of soil air permeability: boundary conditions and measurement scale. *Soil Science.* 166(2), 97-106.

Jabro, J.D., Stevens, W.B., Iversen, W.M., Evans, R.G. (2011). Bulk density, water content, and hydraulic properties of a sandy loam soil following conventional or strip tillage. *Applied engineering in agriculture.* 27(5), 765.

Lai, L., Zhao, X., Jiang, L., Wang, Y., Luo, L., Zheng, Y., Chen, X., & Rimmington, G. M. (2012). Soil respiration in different agricultural and natural ecosystems in an arid region. *PloS one.* 7(10). https://doi.org/10.1371/journal.pone.0048011.

Lin, J., Sun, Y., Schulze Lammers, P. (2014). Evaluating model-based relationship of cone index, soil water content and bulk density using dual-sensor penetrometer data. *Soil and Tillage Research.*138,9-16, ISSN 0167-1987, https://doi.org/10.1016/j.still.2013.12.004.

Łukowska, A., Tomaszuk, P., Dzierżek, K., & Magnuszewski, Ł. (2019). Soil sampling mobile platform for Agriculture 4.0. *2019 20th International Carpathian Control Conference (ICCC),* Krakow-Wieliczka, Poland. doi: 10.1109/CarpathianCC.2019.8765937.

Mohammadi, M. H., Vanclooster, M. (2019). A Simple Device for Field and Laboratory Measurements of Soil Air Permeability. *Soil Science Society of America Journal.* 83(1), 58-63.

Naumov, V.N., Mashkob, K.Y., Byakov, K.E. (2019). Automatic determination of soil parameters by robotic vehicles. *Journal of Physics.: Conference Ser.ies 1177 012016*. Orlando. FL, USA.

Ojo, E. R., Bullock, P. R., L'Heureux, J., Powers, J., McNairn, H., & Pacheco, A. (2015) Calibration and Evaluation of a

Frequency Domain Reflectometry Sensor for Real-Time Soil Moisture Monitoring. *Vadose Zone Journal*. 14(3). https://doi.org/10.2136/vzj2014.08.0114

Payne, P. C. J. (1956) A field method of measuring soil/metal friction. *Journal of Soil Science*, 7, 2.

Rika Corp (2021). RK520-02 Soil Moisture Sensor, Temperature Probe& EC Sensor. From https://www.rikasensor.com/rk520-02-soil-moisture-sensor-temperature-probe-ec-sensor.html

Rossel, R. A., & Bouma, J. (2016). Soil sensing: A new paradigm for agriculture. *Agricultural Systems*. 148, 71-74. doi: 10.1016/j.agsy.2016.07.001

Saffih-Hdadi, K., Défossez, P., Richard, G., Cui, Y.-J., Tang, A.-M., Chaplain, V. (2009). A method for predicting soil susceptibility to the compaction of surface layers as a function of water content and bulk density. *Soil and Tillage Research,* 105(1), 96-103, ISSN 0167-1987, https://doi.org/10.1016/j.still.2009.05.012.

Schirrmann, M., Gebbers, R., Kramer, E., & Seidel, J. (2011). Soil pH Mapping with an On-The-Go Sensor. *Sensors,* 11(1), 573-598. doi:10.3390/s110100573

Scholz, C., Möller, K., Ruckelshausen, A., Hinck, S., & Göttinger, M. (2014). Automatic soil penetrometer measurements and GIS-based documentation with the autonomous field robot platform Bonirob. *12th International Conference on Precision Agriculture.* Sacramento, California, USA.

Seiffert, S., Kaselowsky, J., Jungk, A., Claassen, N. (1995). Observed and Calculated Potassium Uptake by Maize as Affected by Soil Water Content and Bulk Density. *Agronomy Journal,* 87(6), 1070-1077, https://doi.org/10.2134/agronj1995.00021962008700060007x.

Stafford, J. V. (2000). Implementing Precision Agriculture in the 21st Century. *Journal of Agricultural Engineering Research,* 76, 3, 267-275, ISSN 0021-8634, https://doi.org/10.1006/jaer.2000.0577.

Tong, J., Ren, L., Chen, B., & Qaisrani, A. R. (1994). Characteristics of adhesion between soil and solid surfaces. *Journal of Terramechanics*. 31(2), 93-105. https://doi.org/10.1016/0022-4898(94)90009-4.

Ünal, İ., Kabaş, Ö., & Sözer, S. (2020). Real-Time Electrical Resistivity Measurement and Mapping Platform of the Soils with an Autonomous Robot for Precision Farming Applications. *Sensors*. *20(1)*, 251.

USDA (2008). Soil Quality Indicators. USDA Natural Resources Conservation Service. https://www.nrcs.usda.gov/Internet/FSE_DOCUMENTS/nrcs142p2_053261.pdf

Vaz, C.M.P., Bassoi, L.H., Hopmans, J.W. (2001) Contribution of water content and bulk density to field soil penetration

resistance as measured by a combined cone penetrometer–TDR probe. *Soil and Tillage Research.* 60(1–2), 35-42, ISSN 0167-1987, https://doi.org/10.1016/S0167-1987(01)00173-8.

Vaz, C. M. P., Manieri, J. M., de Maria, I. C., & Tuller, M. (2011) Modeling and correction of soil penetration resistance for varying soil water content. *Geoderma,* 166,1(92-101). ISSN 0016-7061, https://doi.org/10.1016/j.geoderma.2011.07.016.

Voorhees, W. B., Farrel, D.A., & Larson, W. E. (1975) Soil Strength and Aeration Effects on Root Elongation. *Soil Science Society of America Journal*, 39(5), 948-953.

Voroney, P. (2019). Chapter 4 - Soils for Horse Pasture Management. *Horse Pasture Management*, Academic Press, Pages 65-79, ISBN 9780128129197, https://doi.org/10.1016/B978-0-12-812919-7.00004-4.

Zhang, N., Wang, M., Wang, N. (2002) Precision agriculture—a worldwide overview. *Computers and Electronics in Agriculture*, 36(2–3), 113-132, ISSN 0168-1699, https://doi.org/10.1016/S0168-1699(02)00096-0.

APPENDIX A: 2D DRAWINGS

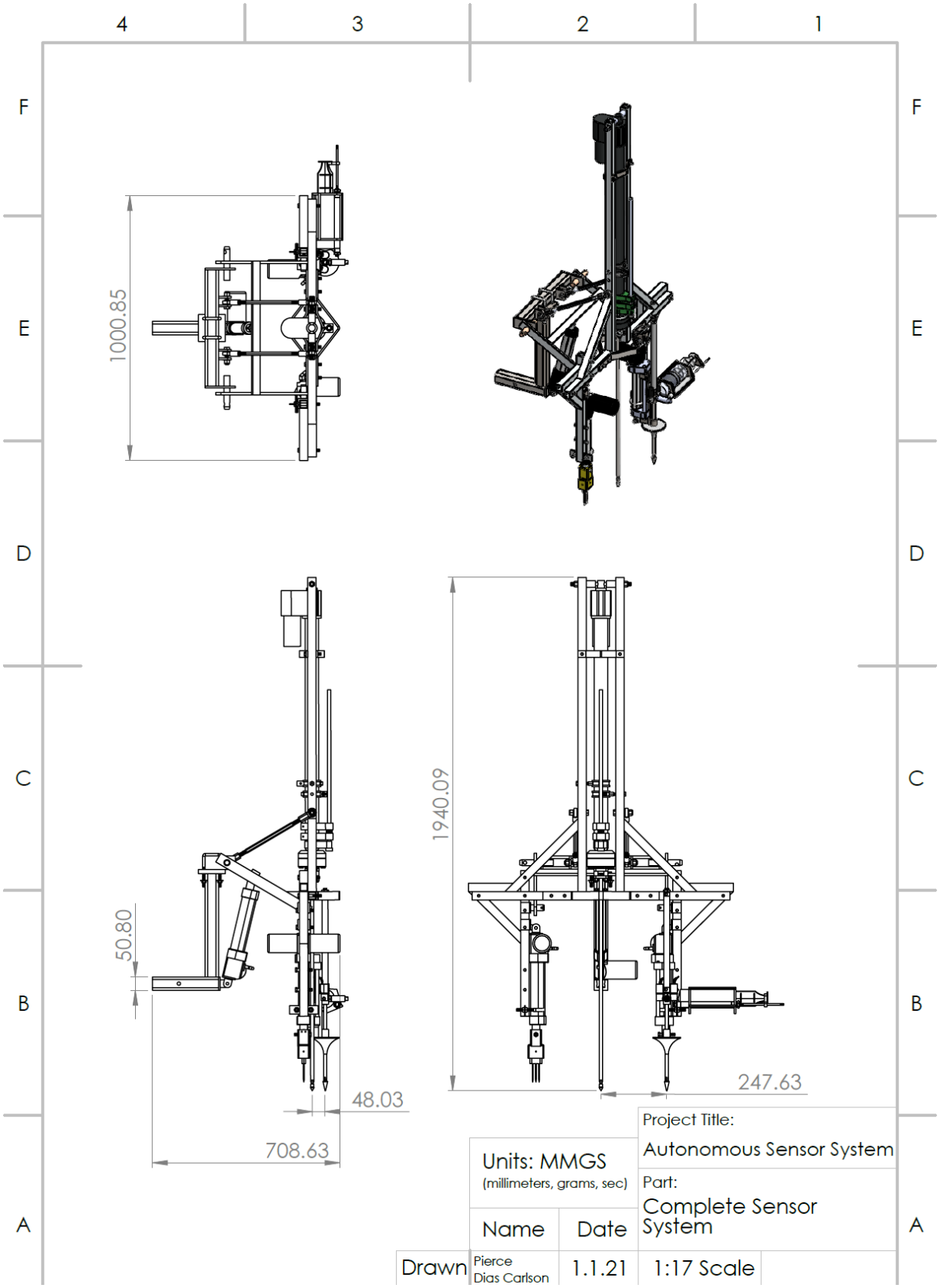

Figure 7.1 2D engineering drawing of sensor system

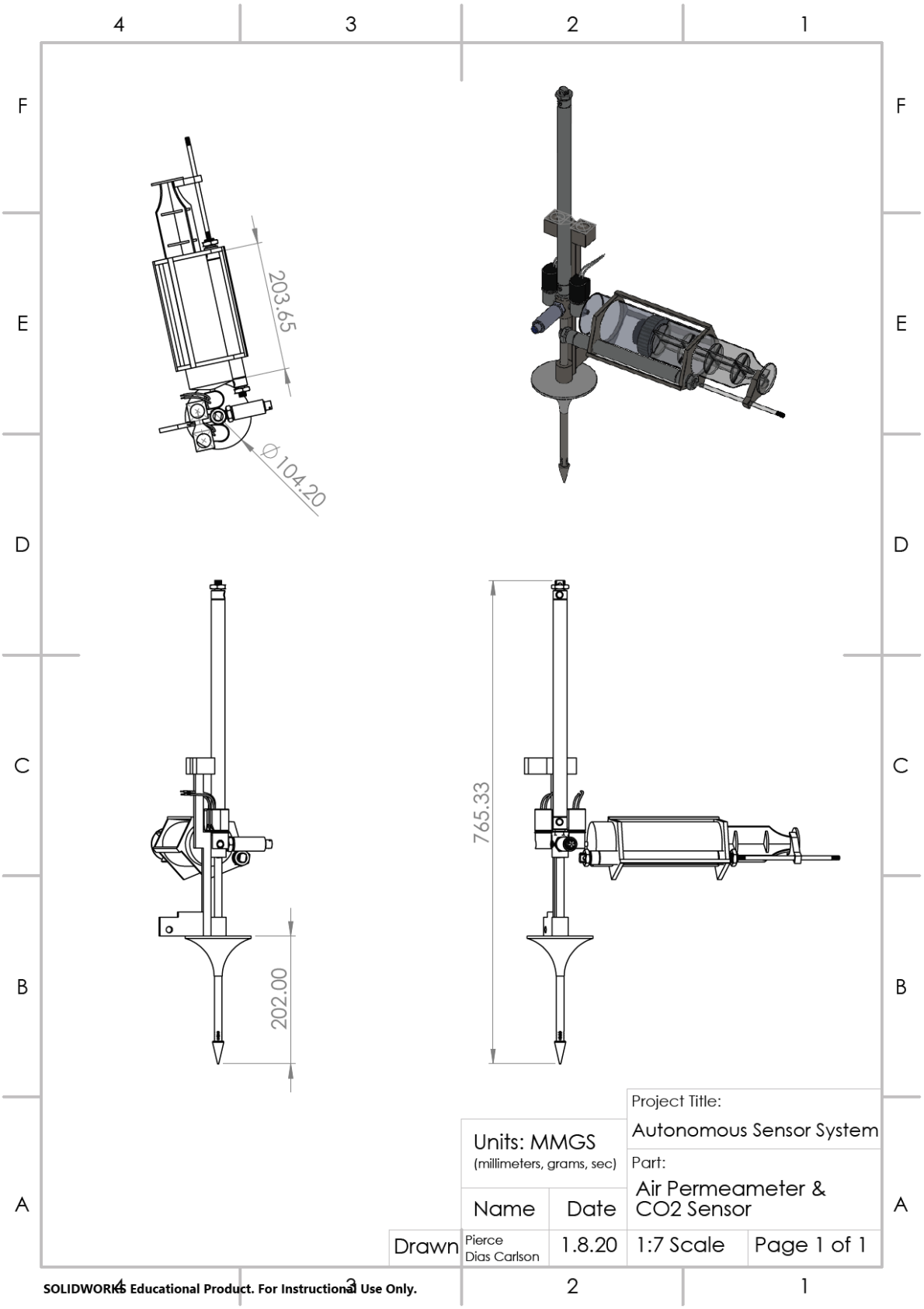

Figure 7.2 2D engineering drawing of air permeameter and CO2 sensor

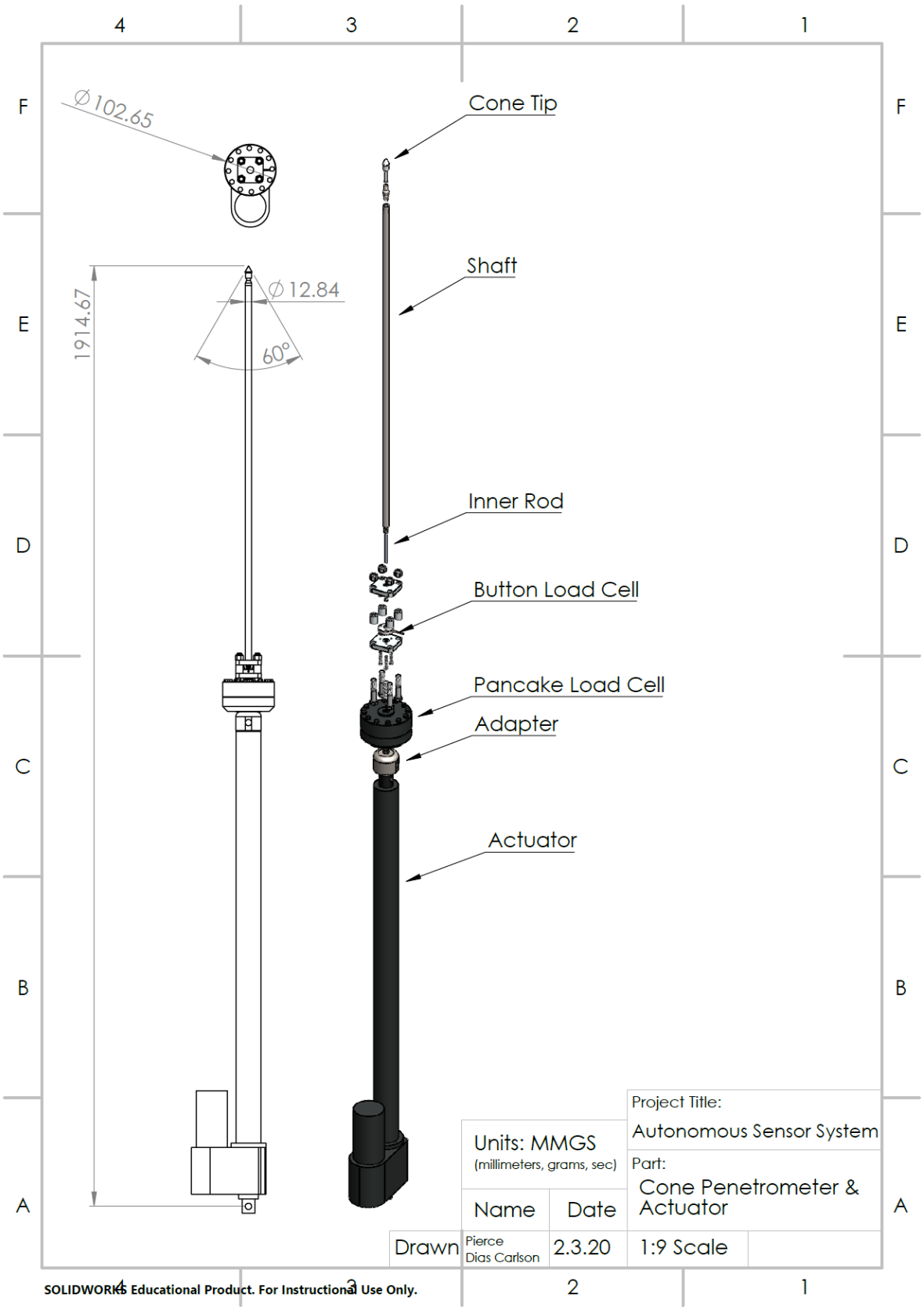

Figure 7.3 2D engineering drawing of Dual Load Cell Penetrometer (DLCP)

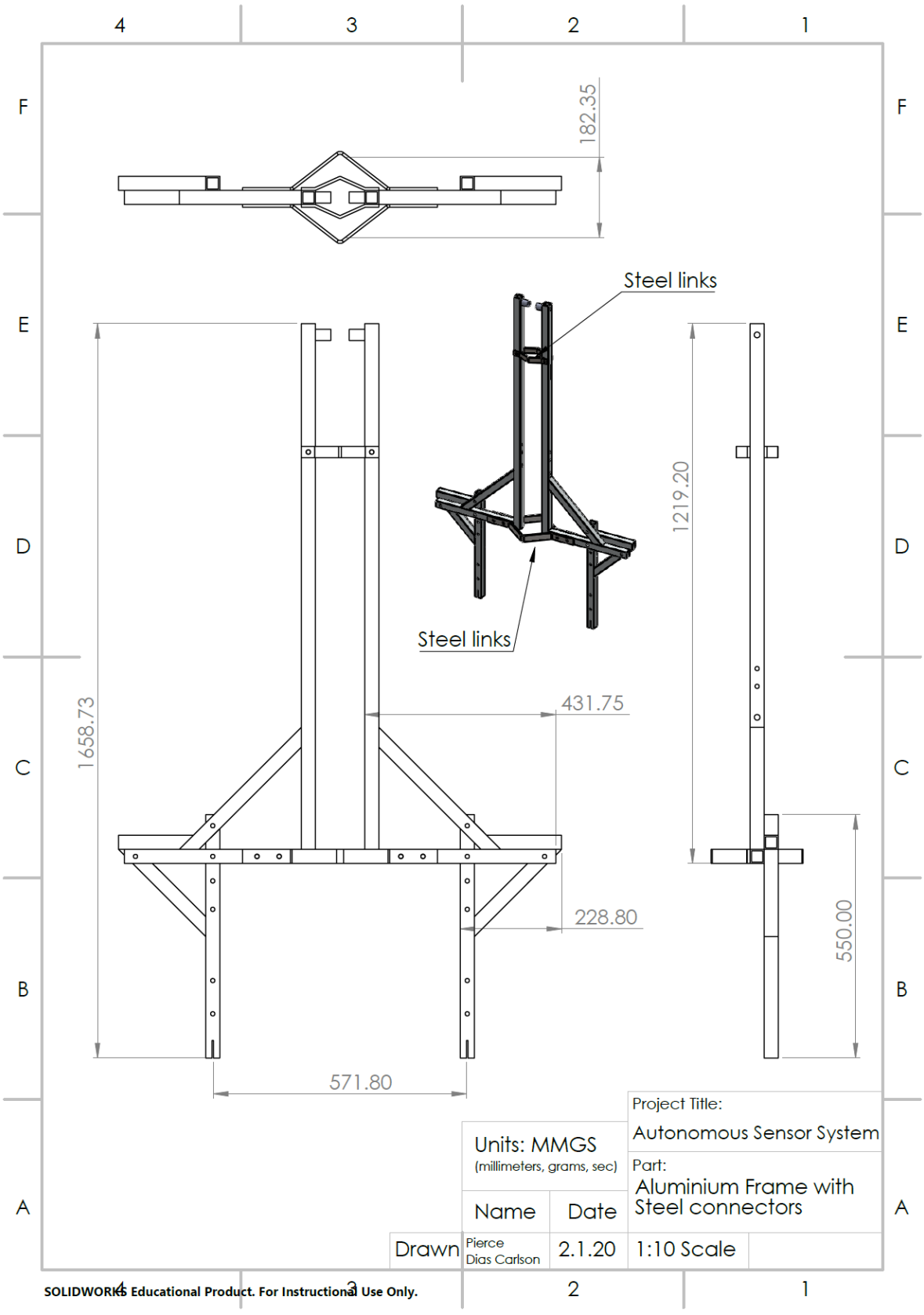

Figure 7.4 2D engineering drawing of main frame

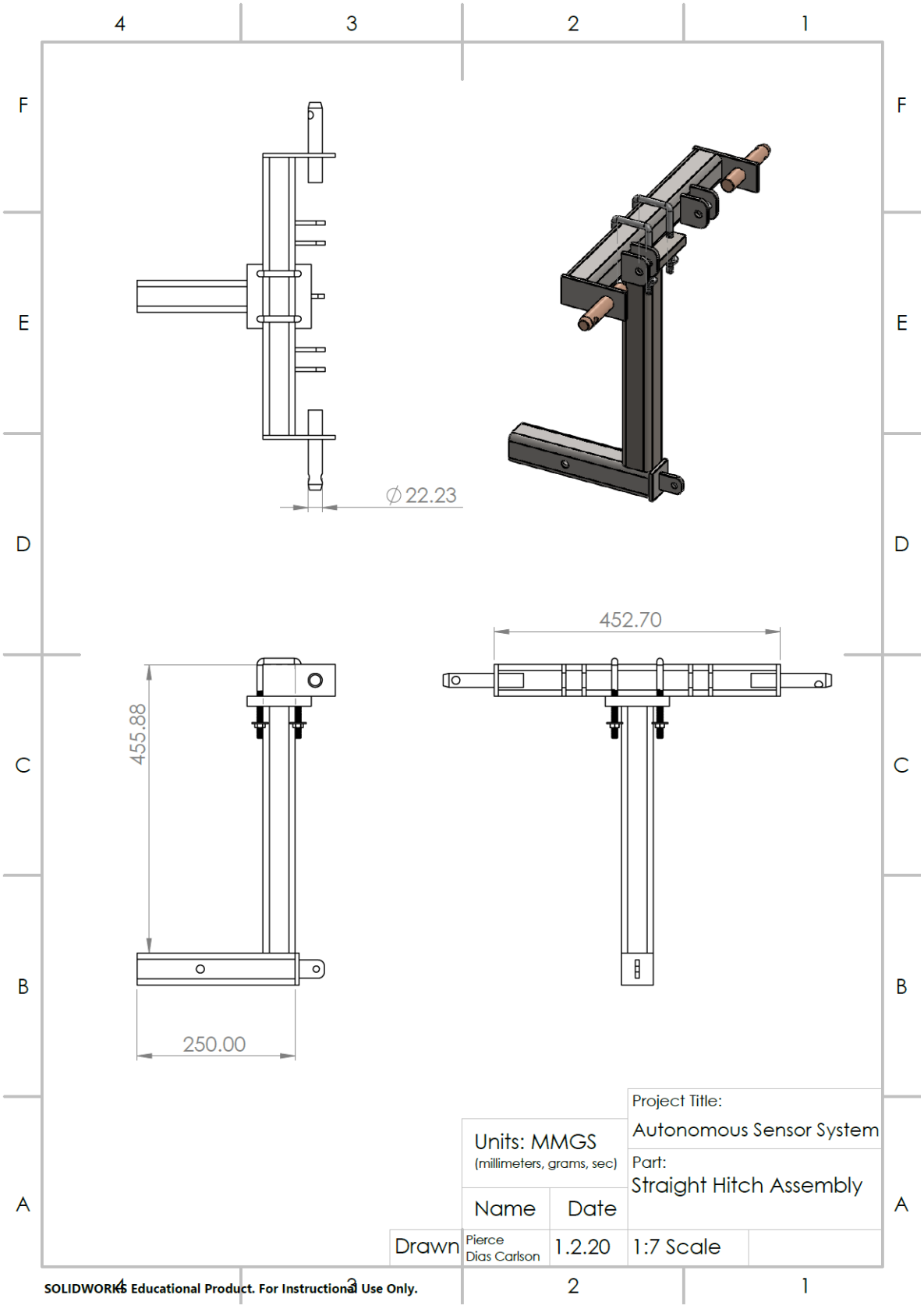

Figure 7.5 2D engineering drawing of straight hitch assembly

APPENDIX B: CODE

Python Code

```
######## Soil Sensor System #########

from time import sleep
from datetime import datetime
import nidaqmx
from nidaqmx.constants import AcquisitionType, TaskMode, CountDirection, Edge
from nidaqmx._task_modules.channels.ci_channel import CIChannel
from nidaqmx._task_modules.channel_collection import ChannelCollection
import serial
import pynmea2
import threading

##################Define Functions
def getDecDigit(digit):
    digits = ['0','1','2','3','4','5','6','7','8','9','A','B','C','D','E','F']
    for x in range(len(digits)):
        if digit == digits[x]:
            return x

def hexToDec(hexNum):           #hex to decimal conversion
    decNum = 0
    power = 0
    for digit in range (len(hexNum), 0, -1):
            decNum = decNum + 16 ** power * getDecDigit(hexNum[digit-1])
            power += 1
    return decNum

def Average(lst):           #average function
    return sum(lst) / len(lst)


# hex string to return data from RK520-02
msg = [0xFE,0x03,0x00,0x00,0x00,0x03,0x11,0xC4]

#gps string
gpsdata = ''

                                                #open RK520-02 serial port
serrk = serial.Serial(
    port='COM6',\
```

```
    baudrate=9600,\
    parity=serial.PARITY_NONE,\
    stopbits=serial.STOPBITS_ONE,\
    bytesize=serial.EIGHTBITS,\
        timeout=0)

                                                    #Open arduino serial port f
or co2

serco2 = serial.Serial(
    port='COM5',\
    baudrate=9600,\
    parity=serial.PARITY_NONE,\
    stopbits=serial.STOPBITS_ONE,\
    bytesize=serial.EIGHTBITS,\
        timeout=0)
                                                # Main Actuator channel creation
Penetrometer_speed = nidaqmx.Task()
Penetrometer_speed.ao_channels.add_ao_voltage_chan("Dev1/ao0")
Penetrometer_direction = nidaqmx.Task()
Penetrometer_direction.ao_channels.add_ao_voltage_chan("Dev1/ao1")

                                                    # Main Actuator Position ch
annel creation
Penetrometer_position = nidaqmx.Task()
Penetrometer_position.ai_channels.add_ai_voltage_chan("Dev1/ai0")

                                                    #Right motor channel creati
on
RightMotorSpeed = nidaqmx.Task()
RightMotorSpeed.do_channels.add_do_chan('Dev1/port0/line0:0')
Right_Motor_Direction = nidaqmx.Task()
Right_Motor_Direction.do_channels.add_do_chan('Dev1/port0/line3:3')

                                                    #Lift Motor channel creatio
n
LiftMotorSpeed = nidaqmx.Task()
LiftMotorSpeed.do_channels.add_do_chan('Dev1/port0/line1:1')
Lift_Motor_Direction  = nidaqmx.Task()
Lift_Motor_Direction.do_channels.add_do_chan('Dev1/port0/line4:4')

                                                    #Left Motor channel creatio
n
LeftMotorSpeed = nidaqmx.Task()
LeftMotorSpeed.do_channels.add_do_chan('Dev1/port0/line2:2')
```

```
Left_Motor_Direction = nidaqmx.Task()
Left_Motor_Direction.do_channels.add_do_chan('Dev1/port0/line5:5')

                                                    #Load Cell - Penetration Re
sistance channel creation
Penetration_resistance = nidaqmx.Task()
Penetration_resistance.ai_channels.add_ai_voltage_chan("Dev1/ai2")

                                                    #Load Cell - Shaft Friction
 channel creation
Shaft_Friction = nidaqmx.Task()
Shaft_Friction.ai_channels.add_ai_voltage_chan("Dev1/ai1")

                                                    #Pressure Transducer channe
l creation
Pressure = nidaqmx.Task()
Pressure.ai_channels.add_ai_voltage_chan("Dev1/ai4")


################## INITIALIZATION ##############################
LiftMotorSpeed.write(True)              #Set all motors to zero position
Lift_Motor_Direction.write(False)
sleep(0.5)
RightMotorSpeed.write(True)
Right_Motor_Direction.write(False)
sleep(0.5)
LeftMotorSpeed.write(True)
Left_Motor_Direction.write(False)
sleep(0.5)
Penetrometer_speed.write(5)
Penetrometer_direction.write(0)

serco2.write('bf \n'.encode('utf_8'))       #cycle air in co2 sensor

sleep(16)
                                           #Turn all motors off
Penetrometer_speed.write(0)
LeftMotorSpeed.write(False)
RightMotorSpeed.write(False)
LiftMotorSpeed.write(False)
                                           #Set Lift motor to moving position
sleep(0.5)
LiftMotorSpeed.write(True)
Lift_Motor_Direction.write(True)
sleep(10)
```

```
LiftMotorSpeed.write(False)




################################## Penetrometer Sequence ########################
########
def conepenetrometer():
    sleep(1)
    l_resistance = []
    profile = 0
    load = 0
    mpa=0
    totalf = 0
    resistance = 0
    Penetrometer_speed.write(2.5)
    Penetrometer_direction.write(5)
                                            # Create Resistance Profile
    f = open("DATA.txt","a")
    while (totalf <= 300.0) & (profile <  20):
        i=0
        potvolt = []
        loadlist = []
        resistancelist = []
        while i < 1:
            potvolt.append(Penetrometer_position.read())
            i += 0.05
            loadlist.append(Penetration_resistance.read())
            resistancelist.append(Shaft_Friction.read())
        load = 500*Average(loadlist)/10.09
        resistance = (1000*(Average(resistancelist)/10.07635))- load
        mpa = (load/0.2325) * 0.00689476
        timestampp1 = datetime.now()            #grab time of measurement
        timestampp = str(timestampp1)[0:19]
        profile = ((Average(potvolt)+0.47) * 13.3333)-1
        l_resistance += ['PT,' + timestampp +','+ gpsdata + str(profile)+',cm,'
 + 'PR,'+ str(mpa)+",MPa,"+'SF,'+str(resistance)+',lb,\n']
    Penetrometer_speed.write(0)
    sleep(1)
    Penetrometer_direction.write(0)
    Penetrometer_speed.write(4)
    f.writelines(l_resistance)  #write data to txt file
    f.close()
    sleep(15)
```

```
    Penetrometer_speed.write(0)


######################### RK Sensor Sequence ###################################
################
def threeprong():
    sleep(20)
    RightMotorSpeed.write(True)
    Right_Motor_Direction.write(True)
    sleep(9)
    RightMotorSpeed.write(False)
    EC_List = []
    Temperature_List = []
    Moisture_List = []
    RK_time = 0.5
    rk_total_time = 0
    rklist = []
    while rk_total_time <= 10:      # take measurements over 10 seconds
        serrk.write(serial.to_bytes(msg))           #write message to sensor
        line = serrk.readline().hex().upper()       #receive sensor data in res
ponse
        rk_total_time += RK_time
        sleep(RK_time)
        timestampr1 = datetime.now()
        timestampr = str(timestampr1)[0:19]
        try:                                        #conversion of string to in
dividual readings
            moisture_hex = str(line[6:10])
            temperature_hex = str(line[10:14])
            EC_hex = str(line[14:18])
            moisture_dec = hexToDec(moisture_hex)
            temperature_dec = hexToDec(temperature_hex)
            EC_dec = hexToDec(EC_hex)
            # if moisture_dec is not None:
            moisture = float(moisture_dec)/100
            # if temperature_dec is not None:
            temperature = float(temperature_dec)/100
            # if EC_dec is not None:
            EC = float(EC_dec)/1000
            rklist.append('RK,' + timestampr +','+ gpsdata + ',EC:,'+str(EC)+',
mS/cm ,Moisture:,'+str(moisture)+',% ,T:,'+str(temperature)+",C,"+'\n')
        except (RuntimeError, TypeError, NameError):
            pass
```

```
    f = open("DATA.txt","a")            #write data to file
    f.writelines(''.join(rklist) )
    f.close()
    sleep(6)
    RightMotorSpeed.write(True)
    Right_Motor_Direction.write(False)
    sleep(11)
    RightMotorSpeed.write(False)

################################CO2 AIR SEQUENCE ##############################
######################

def co2():
    sleep(20)
    LeftMotorSpeed.write(True)
    Left_Motor_Direction.write(True)
    sleep(15)
    LeftMotorSpeed.write(False)
    sleep(1)
    serco2.write('ba \n'.encode('utf_8'))       #open first cylinder
    sleep(5)
    serco2.write('bc \n'.encode('utf_8'))       #open valve and syringe
    sleep(3)
    co2time = 0
    CO2_LIST = []
    timestampc1 = datetime.now()
    timestampc = str(timestampc1)[0:19]
    while co2time <= 11:                        #receive co2 concentrations ove
r serial
        concentrationline = serco2.readline()
        concentration = str(concentrationline[0:5].decode('utf-8'))
        CO2_LIST.append('CO2,' + timestampc +','+ gpsdata + str(concentration)
+ ',mg/kg @ ,'+ str(co2time) + ',s,'+ '\n')
        sleep(0.5)
        co2time += 0.5

    f = open("DATA.txt","a")
    f.writelines(''.join(CO2_LIST) )            #write co2 data to file
    f.close()
    pressuretime = 0.0
    pressurelist = []
    sleep(10)
    serco2.write('bd \n'.encode('utf_8'))       #begin injection
    pressure = 0.0
```

```
    timestampap1 = datetime.now()
    timestampap = str(timestampap1)[0:19]
    while pressuretime <= 5:                    #record injection pressure over
 5s
            pressuretime += 0.05
            pressure = (Pressure.read() - 0.5) * 25
            pressurelist.append('AP,' +timestampap +','+ gpsdata + str(pressure
) + ',psi @ ,' + str(pressuretime) + ',s,'+ '\n')
            sleep(0.05)
    f = open("DATA.txt","a")                    #write pressure data to txt fil
e
    f.writelines(''.join(pressurelist) )
    f.close()

############################## EVENT SEQUENCE ###################################
##########

while True:
    input()
    sleep(1)
    LiftMotorSpeed.write(True)              #set sensor system to measurment po
sition
    Lift_Motor_Direction.write(False)
    sleep(10)
    LiftMotorSpeed.write(False)
    with serial.Serial('COM4', baudrate=38400, timeout=1) as ser:   #receive an
d translate GPS data
        # read 10 lines from the serial output
            for i in range(10):
                line = ser.readline().decode('ascii', errors='replace')
                #print(line)
                if (line.strip()[:6] == '$GPGGA'):
                    nmea = line.strip()
                    nmeaobj = pynmea2.parse(str(nmea))
                    #print(nmeaobj)
                    gpsdata = str(nmeaobj.timestamp) + ','+ str(nmeaobj.lat) +
str(nmeaobj.lat_dir) + ',' + str(nmeaobj.lon) + str(nmeaobj.lon_dir) + ',' + st
r(nmeaobj.altitude) + ',' #. . true_coursedirection #.heading
                    print(gpsdata)
                                                        # Lift
    p1 = threading.Thread(target=conepenetrometer)      #create threads
    p2 = threading.Thread(target=threeprong)
    p3 = threading.Thread(target=co2)
    p1.start()                                  #start threads
    p2.start()
```

```
    p3.start()
    p1.join()                                   #join threads
    p2.join()
    p3.join()
    LeftMotorSpeed.write(True)                  #when threads finish, retract actua
tor
    Left_Motor_Direction.write(False)
    sleep(18)
    LeftMotorSpeed.write(False)
    sleep(2)
    serco2.write('be \n'.encode('utf_8'))
    ###################Return to Travel Position
    if Penetrometer_position.read() < 0.05:         #check penetrometer is retr
acted
        LiftMotorSpeed.write(True)
        Lift_Motor_Direction.write(True)
        sleep(11)
        LiftMotorSpeed.write(False)
    else:                                           #if not, retract
        Penetrometer_speed.write(4)
        Penetrometer_direction.write(0)
        sleep(15)
        Penetrometer_speed.write(0)
        LiftMotorSpeed.write(True)
        Lift_Motor_Direction.write(True)
        sleep(11)
        LiftMotorSpeed.write(False)
```

Arduino Code

```
#include <Keyboard.h>

String inData;
String val= "";
double co2 =0;
double multiplier = 1;
uint8_t buffer[25];
uint8_t ind =0;

void setup() {
```

```
  int injection = 8;
  int syringevalve = 9;
  int syringe = 10;
  int largesyringe = 11;
pinMode(8, OUTPUT);
pinMode(9, OUTPUT);
pinMode(10, OUTPUT);
pinMode(11, OUTPUT);
Serial.begin(9600);
Serial1.begin(9600);
digitalWrite(8, HIGH);
digitalWrite(9, HIGH);
digitalWrite(10, HIGH);
digitalWrite(11, LOW);

}

void loop() {

if(Serial.available() > 0) {
  String inChar = Serial.readString();



  if(inChar.indexOf('a') >= 1) {
// Sequence(

digitalWrite(11, HIGH); // OPEN LARGE ACTUATOR
delay(2000);
digitalWrite(9,LOW); // OPEN SYRINGE VALVE
digitalWrite(10, LOW); //OPEN SYRINGE
delay(5000);
digitalWrite(9, HIGH); //CLOSE SYRINGE VALVE
  }


  if(inChar.indexOf('c') >= 1) {
for (int i = 0; i < 25; i++){
// reads co2 and sends to usb-serial
while(buffer[ind-1] != 0x0A)
{
if(Serial1.available())
{
buffer[ind] = Serial1.read();
```

```
ind++;
}
}
report();
}}

if(inChar.indexOf('d') >= 1) {

digitalWrite(8, LOW); //INJECT AIR
delay(5000);
digitalWrite(8,HIGH); //CLOSE INJECTION
delay(50);

  }
if(inChar.indexOf('e') >= 1) {
  digitalWrite(9,LOW); //OPEN SYRINGE VALVE
digitalWrite(10,HIGH); //CLOSE SYRINGE
delay(3000);
    digitalWrite(8, LOW); // INJECT AIR

delay(1000);
digitalWrite(8,HIGH);
digitalWrite(11, LOW); //CLOSE LARGE ACTUATOR
digitalWrite(9,HIGH); //CLOSE SYRINGE VALVE}
  }

if(inChar.indexOf('f') >= 1) {
    digitalWrite(11, HIGH); // OPEN LARGE ACTUATOR
    delay(2000);
digitalWrite(9,LOW); //OPEN SYRINGE VALVE
digitalWrite(10,HIGH); //CLOSE SYRINGE
delay(3000);
digitalWrite(10,LOW); //OPEN SYRINGE
delay(3000);
digitalWrite(10,HIGH); //CLOSE SYRINGE
delay(3000);
digitalWrite(10,LOW); //OPEN SYRINGE
delay(3000);
digitalWrite(10,HIGH); //CLOSE SYRINGE
delay(5000);
digitalWrite(9,HIGH); //CLOSE SYRINGE VALVE
digitalWrite(11, LOW); //CLOSE LARGE ACTUATOR
  }

if(inChar.indexOf('g') >= 1) {
```

```
  digitalWrite(11, HIGH); // OPEN LARGE ACTUATOR
digitalWrite(9,LOW); //OPEN SYRINGE VALVE

  }
}}

void report()
{
for(int i=0; i < ind+1; i++)
{
if(buffer[i] == 'z')
break;
if((buffer[i] != 0x5A)&&(buffer[i] != 0x20))
{
val += buffer[i]-48;

}
}
co2 = val.toInt();

Serial.print(co2);
Serial.println();
ind=0;
val="";
}
```

APPENDIX C: DATA

Dataset 1

Measurement ID	Elevation	RK520 EC	RK520 VWC	RK520 T	PR Shallow	PR Deep	SMF Deep	Air Pressure 1-4	Veris EC
1	34.465	0.231	30.35	14.22	.	.	.	.	2.10
2	35.043	0.296	20.72	12.44	1.33	1.84	11.88	3.70	2.08
3	35.043	0.275	35	11.82	1.69	1.40	8.48	7.13	2.08
4	38.275	0.032	18.91	11.93	1.99	1.75	5.26	7.84	0.98
5	38.632	0.087	34.09	11.31	1.07	1.40	6.30	7.57	1.83
6	38.676	0.071	31.75	12.15	1.13	1.26	6.20	.	1.40
7	38.694	0.084	28.95	11.84	1.34	1.36	6.39	4.42	1.21
8	37.787	0.075	28.75	11.41	1.72	1.79	6.22	.	0.89
9	37.864	0.067	32.64	11.16	1.34	1.48	5.65	.	0.99
10	38.365	0.059	29.87	11.27	1.36	1.74	6.37	3.50	0.99
11	36.582	0.097	32.44	11.62	1.41	1.54	7.16	8.23	1.19
12	35.769	0.063	28.53	11.27	1.25	2.28	4.62	2.21	0.79
13	34.772	0.144	37.04	11.01	1.18	1.47	9.70	5.88	2.40
14	35.525	0.063	24.81	10.79	1.27	1.36	7.00	.	1.56
15	35.733	0.073	18.04	12.63	1.41	1.81	6.73	2.15	1.66
16	35.556	0.063	29.79	10.68	1.54	1.51	7.28	1.83	1.37
17	35.175	0.108	28.27	11.37	1.37	1.22	9.02	5.78	2.32
18	36.266	0.047	22.47	11.09	1.86	2.49	10.61	4.78	1.46
19	37.34	0.085	33.33	11.19	1.46	1.49	4.65	7.49	1.01
20	37.921	0.052	28.96	11.31	1.01	1.37	6.37	.	1.01
21	37.935	0.072	35.67	10.58	1.28	1.32	6.25	6.72	1.01
22	35.853	0.039	29.62	11.3	1.05	1.36	9.11	4.60	0.80
23	36.904	0.071	31.05	10.68	0.97	1.15	8.90	4.69	1.06
24	34.433	0.104	28.91	10.68	1.23	1.40	11.88	7.12	2.60
25	35.299	0.155	30.22	11.22	1.22	1.38	.	6.44	3.86
26	35.738	0.135	36.13	11.08	1.39	1.81	4.70	6.33	2.69
27	35.852	0.079	31.37	10.89	1.26	1.63	4.67	5.11	1.03
28	35.914	0.046	24.92	10.76	1.37	1.56	10.87	.	1.22
29	35.905	0.048	24.13	10.44	1.29	1.30	10.34	4.03	1.47
30	36.881	0.088	28.64	11.2	1.22	1.47	.	4.06	2.42
31	34.735	0.103	29.86	10.9	1.33	1.79	12.32	6.77	2.80
32	35.146	0.171	32.44	10.68	.	.	.	9.19	3.58
33	35.641	0.213	36.78	10.78	1.42	1.29	10.98	8.66	3.54
34	40.402	0.112	32.48	10.86	1.66	1.69	7.61	8.48	3.82
35	40.402	0.251	32.45	10.79	.	.	.	6.09	3.82

Dataset 2

ID	BD	RK520 VWC	RK520 T	RK520 EC	FS VWC	FS T	FS EC	GWC	VWC	AP 1-4	AP 1-2	AP 2-4	AP Ratio	PR Shallow	PR Deep	SMF Shallow	SMF Deep	SMF Ratio	PR Ratio
1	1.25	34.53	11	335.78	27	10.5	408	24.02	29.9	37.30	6.42	5.25	1.22	1.08	1.18	1.94	2.28	0.85	0.91
3	1.27	30.12	11.18	122.16	28.7	11.5	232	21.35	27.11	33.31	5.13	4.86	1.06	1.01	1.33	1.27	1.37	0.93	0.76
4	1.26	17.69	13.05	22.79	18.2	9.9	133	17.99	22.69	13.40	1.94	1.91	1.02	2.28	2.24	1.64	1.04	1.59	1.02
5	1.29	14.76	12.36	269.66	25.4	10.4	191.9	20.6	26.6	18.47	2.67	2.75	0.97	1.10	1.50	1.30	1.08	1.21	0.74
6	1.26	28.48	13.01	108.14	28.2	10.8	173.9	23.41	29.53	27.76	4.21	4.04	1.04	0.73	1.06	1.93	0.86	2.23	0.69
7	1.25	25.37	14.38	52.66	26.5	11.2	101.6	21.82	27.34	40.93	6.21	5.90	1.05	1.25	1.30	2.40	1.14	2.10	0.96
8	1.37	22.06	14.96	38.94	30.9	10.2	161.8	22.94	31.38	20.75	2.82	3.08	0.92	1.40	1.47	2.81	1.26	2.23	0.95
9	1.3	19.61	15.39	63.02	30.9	10.7	144.8	20.12	26.19	41.36	6.40	5.90	1.08	1.18	1.61	2.27	1.00	2.28	0.73
10	1.4	16.42	15.35	19.83	27.3	10.7	128.7	19.9	27.84	.	.	.	.	1.80	2.23	2.09	0.98	2.14	0.81
11	1.34	29.02	12.85	114.27	27.3	12.8	202	21.62	28.88	42.57	6.45	6.20	1.04	1.41	1.48	2.39	1.26	1.89	0.95
12	1.32	22.39	14.01	77.02	35.7	11.5	342	21.14	27.91	46.41	7.21	6.70	1.08	1.10	1.47	2.63	2.01	1.31	0.75
13	1.27	28.21	12.77	184	32.9	10.6	152.8	21.91	27.73	39.96	5.99	5.82	1.03	1.21	1.18	2.37	1.56	1.52	1.03
14	1.25	17.55	16.17	80.84	31.8	10.7	68.6	22.56	28.18	31.16	4.72	4.45	1.06	1.47	1.79	2.71	1.17	2.31	0.82
15	1.27	29.84	15.13	106.7	29	11.7	147.5	22.7	28.76	44.41	6.73	6.51	1.03	1.23	1.14	2.64	1.94	1.36	1.08
16	1.22	23.32	16.34	100.36	35.1	11.5	300.8	22.74	27.76	51.70	8.45	7.33	1.15	1.12	1.22	2.51	2.45	1.03	0.92
17	1.1	24.66	16.16	84.34	35.1	11.6	220	23.51	25.93	48.72	7.61	7.01	1.08	1.15	1.03	2.95	2.35	1.25	1.12
18	1.32	30.81	13.21	101.97	28.4	11.5	90.6	22.08	29.23	50.19	7.81	7.24	1.08	1.12	1.25	2.32	1.53	1.51	0.90
19	1.28	22.08	17.52	32.71	28.4	12.1	119.3	21.28	27.21	21.47	3.53	3.02	1.17	1.33	1.68	1.73	0.76	2.28	0.79
20	1.43	22.2	16.85	40.99	28.4	13.5	55.8	18.27	26.13	19.94	3.03	2.83	1.07	1.08	1.45	1.64	0.87	1.89	0.74
21	1.32	25.38	15.16	98.37	29.8	13.2	223	21.9	29.01	50.82	7.27	7.43	0.98	1.38	1.45	2.72	2.31	1.18	0.95
22	1.06	11.31	13.4	.	28.7	14.2	377	24.85	26.36	27.80	3.95	4.17	0.95	0.86	0.97	2.30	2.14	1.07	0.88
23	1.07	20.55	15.01	.	32.6	12.6	310	22.69	24.22	60.38	9.67	8.71	1.11	1.46	1.47	2.94	3.15	0.93	0.99
24	1.23	31.56	14.28	141.45	32.6	12.6	330	21.89	26.82	65.45	11.00	9.40	1.17	1.46	1.31	3.07	2.98	1.03	1.12
25	1.45	.	12.42	277.63	26.8	13.6	124.4	18.58	26.97	24.72	3.26	3.46	0.94	1.44	2.00	1.54	1.53	1.00	0.72
27	1.27	19.61	14.75	.	22	13.4	209	21.92	27.8	.	.	.	.	1.27	1.10	2.55	2.07	1.23	1.16
28	1.21	17.26	15.14	23.36	28.2	13.5	106.9	22.92	27.76	41.09	5.41	5.99	0.90	1.22	1.19	2.29	1.62	1.41	1.03
29	1.15	22.51	15.69	95.38	15.6	16.8	106.7	22.2	25.46	62.23	9.30	9.04	1.03	1.09	1.63	2.21	1.73	1.28	0.67
30	1.2	16.36	15.57	47.52	15.6	16.5	303	21.74	26.12	32.73	4.51	4.84	0.93	1.45	1.45	2.83	2.44	1.16	1.00
31	1.17	19.2	16.12	156.82	15.9	16.4	297	23.44	27.47	20.49	2.77	3.05	0.91	1.31	1.63	2.89	2.28	1.27	0.81
32	1.42	29.89	15.55	128.56	18.7	16.4	192.8	20.51	29.2	46.47	7.35	6.70	1.10	1.39	1.48	2.44	1.70	1.44	0.94
33	1.26	25.89	15.61	121.77	18.7	15.4	279	21.37	26.99	.	.	.	.	1.32	1.47	2.41	2.41	1.00	0.90
34	1.36	18.48	14.7	77.09	23.7	14.4	408	19.52	26.59	38.51	5.97	5.46	1.09	1.36	1.65	2.45	1.57	1.56	0.83
35	1.36	25.22	13.9	.	21.2	13.5	62.7	21.56	29.29	48.50	7.26	7.03	1.03	1.52	1.64	2.59	1.37	1.89	0.93
36	1.17	27.7	15.82	.	18.4	13.5	141.4	20.01	23.35	24.44	3.41	3.60	0.95	1.25	1.33	1.88	1.25	1.50	0.94
37	1.54	.	.	.	10	7.4	113.3	15.55	23.9	.	.	.	.	2.21	.	3.44	.	.	.
38	1.42	23.26	7.76	57	10.1	6.7	146.1	19.53	27.82	.	.	.	.	2.15	4.56	1.12	3.59	0.31	0.47
39	1.19	31.95	7.31	109	11.5	7	142.6	21.22	25.19	.	.	.	.	0.87	1.42	0.71	1.49	0.47	0.61
40	1.46	23.97	9.07	66	11	7	96.7	17.38	25.42	46.78	7.18	6.72	1.07	1.31	2.13	1.38	1.02	1.35	0.62
41	1.29	24.91	10.12	88	13.7	6.2	180.1	20.55	26.59	28.12	4.47	3.97	1.13	1.09	1.29	1.67	1.11	1.50	0.84
42	1.42	23.94	10.36	64	10.9	8.2	96.3	18.58	26.39	27.48	4.02	4.00	1.00	2.07	1.79	3.25	1.28	2.54	1.16
43	1.27	19.48	12.65	44	9.4	7.5	143.1	.	.	10.23	1.44	1.50	0.96	1.03	1.85	1.52	1.22	1.25	0.56
44	1.37	28.25	10.75	142	13.4	7.9	171.6	18.12	24.82	31.27	4.84	4.50	1.08	1.47	1.80	2.23	1.74	1.28	0.82

APPENDIX D: RENDERS

Figure 10.1 Bearcub 24 and sensor system in travelling position

Figure 10.2 Bearcub 24 and sensor system in measurement position

Figure 10.3 Sensor system with prototype plastic ground plate